Министерство науки и высшего образования Российской Федерации
ФЕДЕРАЛЬНОЕ ГОСУДАРСТВЕННОЕ АВТОНОМНОЕ ОБРАЗОВАТЕЛЬНОЕ УЧРЕЖДЕНИЕ ВЫСШЕГО ОБРАЗОВАНИЯ
НАЦИОНАЛЬНЫЙ ИССЛЕДОВАТЕЛЬСКИЙ УНИВЕРСИТЕТ ИТМО
ITMO University

ВЫПУСКНАЯ КВАЛИФИКАЦИОННАЯ РАБОТА
GRADUATION THESIS

Интерференция коллективных мод в цепочках диэлектрических резонаторов с одновременным электрическим и магнитным дипольным откликом / Interference of Collective Modes in Chains of Dielectric Resonators with Simultaneous Electric and Magnetic Dipolar Responses

Обучающийся / Student Полева Мария Андреевна
Факультет/институт/кластер/ Faculty/Institute/Cluster физический факультет
Группа/Group Z42761
Направление подготовки/ Subject area 16.04.01 Техническая физика
Образовательная программа / Educational program Техническая физика / Physics and engineering 2021
Язык реализации ОП / Language of the educational program Русский, Английский
Статус ОП / Status of educational program МОП
Квалификация/ Degree level Магистр
Руководитель ВКР/ Thesis supervisor Савельев Роман Сергеевич, кандидат физико-математических наук, Университет ИТМО, физический факультет, доцент (квалификационная категория "ординарный доцент")

Министерство науки и высшего образования Российской Федерации
ФЕДЕРАЛЬНОЕ ГОСУДАРСТВЕННОЕ АВТОНОМНОЕ ОБРАЗОВАТЕЛЬНОЕ УЧРЕЖДЕНИЕ ВЫСШЕГО ОБРАЗОВАНИЯ
НАЦИОНАЛЬНЫЙ ИССЛЕДОВАТЕЛЬСКИЙ УНИВЕРСИТЕТ ИТМО
ITMO University

ЗАДАНИЕ НА ВЫПУСКНУЮ КВАЛИФИКАЦИОННУЮ РАБОТУ / OBJECTIVES FOR A GRADUATION THESIS

Обучающийся / Student Полева Мария Андреевна
Факультет/институт/кластер/ Faculty/Institute/Cluster физический факультет
Группа/Group Z42761
Направление подготовки/ Subject area 16.04.01 Техническая физика
Образовательная программа / Educational program Техническая физика / Physics and engineering 2021
Язык реализации ОП / Language of the educational program Русский, Английский
Статус ОП / Status of educational program МОП
Квалификация/ Degree level Магистр
Тема ВКР/ Thesis topic Интерференция коллективных мод в цепочках диэлектрических резонаторов с одновременным электрическим и магнитным дипольным откликом / Interference of collective modes in chains of dielectric resonators with simultaneous electric and magnetic dipolar responses
Руководитель ВКР/ Thesis supervisor Савельев Роман Сергеевич, кандидат физико-математических наук, Университет ИТМО, физический факультет, доцент (квалификационная категория "ординарный доцент")

Основные вопросы, подлежащие разработке / Key issues to be analyzed
1. Thesis requirements:
To develop an experimental design of the chain of the dielectric resonators with simultaneous magnetic and electric dipole responses that support collective states with high quality factors, analyze radiation patterns and find appropriate conditions for excitation of such states.

2. Contents:
2. 1. Theoretical dipole model that allows for the calculation of the characteristics of infinite and finite chains of the scatterers supporting electric and magnetic dipole resonances.
2. 2. Search for the parameters of the scatterers that correspond to the formation of collective modes with increased quality factors due to mode interference.
2.3. Design of realistic systems with parameters found in p.2. Calculation of their characteristics.

3. Goal and tasks of the project list of key issues to be analyzed:

3.1. Development of a theoretical model describing the chain of scatterers with simultaneous magnetic and electric dipole responses.
3.2. Analysis of dispersion curves of the infinite chain of scatterers within the framework of the dipole model developed in 1.
3.3. Search for the parameters, for which the dispersion becomes non-monotonic, allowing for the achievement of destructive interference of the collective modes with close frequencies.

3.4. Analysis of the behavior of the finite systems with the parameters found in 3. Calculation of the dependence of the quality factors on the period and the number of particles.

3.5. Using numerical fit, the determination of the parameters of the realistic scatterers based on the parameters obtained within the framework of the dipole model.

3.6. Calculation of the scattering cross-section for the realistic designs using 2D and 3D models in COMSOL Multiphysics. Analysis of the results and extraction of the eigenfrequencies and quality factors from the spectral response.

3.7. Calculation of the radiation patterns of the collective modes in the finite systems within the framework of the dipole model and in COMSOL Multiphysics for the realistic dielectric scatterers. Investigation of the dependence of the shape of the radiation patterns on the quality factor of the mode in both cases.

4. Recommended materials and sourcebooks for completion of thesis:

4.1. Kornovan D. F. et al. High-Q localized states in finite arrays of subwavelength resonators //ACS Photonics. – 2021. – T. 8. – №. 12. – C. 3627-3632.

4.2. Sirmaci Y. et al. All-dielectric Huygens' meta-waveguides for resonant integrated photonics. – 2022.

4.3. Figotin A., Vitebskiy I. Gigantic transmission band-edge resonance in periodic stacks of anisotropic layers //Physical review E. – 2005. – T. 72. – №. 3. – C. 036619.

4.4. Rutckaia V. et al. Coupling of germanium quantum dots with collective sub-radiant modes of silicon nanopillar arrays //Acs Photonics. – 2020. – T. 8. – №. 1. – C. 209-217.

4.5. Hoang T. X. et al. Collective Mie resonances for directional on-chip nanolasers //Nano Letters. – 2020. – T. 20. – №. 8. – C. 5655-5661.

Дата выдачи задания / Assignment issued on: 15.01.2023

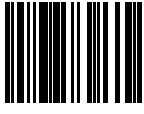**Срок представления готовой ВКР / Deadline for final edition of the thesis** 20.06.2023

Характеристика темы ВКР / Description of thesis subject (topic)

Тема в области фундаментальных исследований / Subject of fundamental research: да / yes

Тема в области прикладных исследований / Subject of applied research: нет / not

СОГЛАСОВАНО / AGREED:

Руководитель ВКР/ Thesis supervisor	Документ подписан		Савельев Роман Сергеевич
	Савельев Роман Сергеевич		
	10.03.2023		
	(эл. подпись)		

Задание принял к исполнению/ Objectives assumed BY	Документ подписан		Полева Мария Андреевна
	Полева Мария Андреевна		
	17.03.2023		
	(эл. подпись)		

Руководитель ОП/ Head
of educational program

Белов Павел
Александрович

АННОТАЦИЯ
ВЫПУСКНОЙ КВАЛИФИКАЦИОННОЙ РАБОТЫ
SUMMARY OF A GRADUATION THESIS

Обучающийся / Student Полева Мария Андреевна
Факультет/институт/кластер/ Faculty/Institute/Cluster физический факультет
Группа/Group Z42761
Направление подготовки/ Subject area 16.04.01 Техническая физика
Образовательная программа / Educational program Техническая физика / Physics and engineering 2021
Язык реализации ОП / Language of the educational program Русский, Английский
Статус ОП / Status of educational program МОП
Квалификация/ Degree level Магистр
Тема ВКР/ Thesis topic Интерференция коллективных мод в цепочках диэлектрических резонаторов с одновременным электрическим и магнитным дипольным откликом / Interference of Collective Modes in Chains of Dielectric Resonators with Simultaneous Electric and Magnetic Dipolar Responses
Руководитель ВКР/ Thesis supervisor Савельев Роман Сергеевич, кандидат физико-математических наук, Университет ИТМО, физический факультет, доцент (квалификационная категория "ординарный доцент")

ХАРАКТЕРИСТИКА ВЫПУСКНОЙ КВАЛИФИКАЦИОННОЙ РАБОТЫ
DESCRIPTION OF THE GRADUATION THESIS

Цель исследования / Research goal
Изучить влияние взаимодействия электрических и магнитных диполей в цепочке диэлектрических резонаторов на поведение дисперсии в бесконечных цепочках и добротности мод в конечных цепочках / To study the influence of the interaction between electric and magnetic dipoles in a chain of dielectric resonators on the behavior of the dispersion in infinite chains and the Q-factor of modes in finite chains

Задачи, решаемые в ВКР / Research tasks
Бесконечная цепочка резонаторов: 1. Вывод уравнения, описывающего электромагнитные свойства бесконечной цепочки диэлектрических резонаторов, которые можно заменить перпендикулярными друг другу магнитным и электрическим диполями. 2. Аппроксимация магнитной и электрической поляризуемостей аналитическими функциями от частоты. 3. Написание кода для решения уравнения из п.1, используя п.2. 4. Построение дисперсий по написанному коду для разных соотношений резонансных частот магнитного и электрического диполя одиночного резонатора. 5. Анализ качественных изменений в поведении дисперсий при изменении соотношения частот. 6. Сравнение результатов, полученных в рамках дипольной модели, с результатами, полученными при помощи полноволнового пакета моделирования. Конечная цепочка резонаторов: 1. Вывод

уравнения, описывающего электромагнитные свойства конечной цепочки диэлектрических резонаторов, используя ранее выведенные аналитические выражения для поляризуемостей. 2. Написание кода для решения уравнения из п.1. 3. Построение зависимости добротности мод от периода структуры для различного числа составляющих цепочки. 4. Построение зависимости добротности от числа частиц в системе для разного соотношения резонансных частот. 5. Сравнение результатов, полученных в рамках дипольной модели, с результатами, полученными при помощи полноволнового пакета моделирования. / An infinite chain of resonators: 1. Derivation of an equation describing the electromagnetic properties of an infinite chain of dielectric resonators, which can be modelled by magnetic and electric dipoles perpendicular to each other. 2. Approximation of magnetic and electric polarizabilities by analytic functions of frequency. 3. Writing code to solve the equation from 1 using 2. 4. Plotting of dispersions according to the written code for different ratios of the resonant frequencies of the magnetic and electric dipole of a single resonator. 5. Analysis of qualitative changes in the behavior of dispersions with a change in the frequency ratio. 6. Comparison of the results obtained in the framework of the dipole model with the results of full-wave simulations. Finite chain of resonators: 1. Derivation of an equation describing the electromagnetic properties of a finite chain of dielectric resonators, using the previously derived analytical expressions for polarizabilities. 2. Writing code for solving the equation from 1. 3. Plotting the dependence of the quality factor of the modes on the period of the structure for a different number of chain components. 4. Construction of the dependence of the quality factor on the number of particles in the system for different ratios of resonant frequencies. 5. Comparison of the results obtained in the framework of the dipole model with the results of full-wave simulations.

Краткая характеристика полученных результатов / Short summary of results/findings
1. Получены уравнение, описывающие электромагнитные свойства бесконечной и конечной цепочек диэлектрических резонаторов, которые можно заменить перпендикулярными друг другу магнитным и электрическим диполями. 2. Получена аппроксимация магнитной и электрической поляризуемостей аналитическими функциями от частоты. 3. Написан код для решения уравнения на собственные значения в конечной и бесконечной цепочках резонаторов. 4. Изучено влияния взаимодействия двух видов диполей на дисперсии и добротности мод. 5. Сравнение результатов , полученных в рамках дипольной модели, с результатами, полученными при помощи полноволнового пакета моделирования, подтвердило правильность используемых моделей. 1. An equation that describes the electromagnetic properties of infinite and finite chains of dielectric resonators, which can be replaced by magnetic and electric dipoles perpendicular to each other, is obtained. 2. An approximation of the magnetic and electric polarizabilities by analytic functions of frequency is obtained. 3. A code for solving the equation for eigenvalues in finite and infinite chains of resonators has been written. 4. The influence of the interaction of two types of dipoles on the dispersion and quality factor of the modes has been studied. 5. Comparison of the results obtained in the framework of the dipole model with the results of full-wave simulations confirmed the correctness of the developed models.

Наличие выступлений на конференциях по теме выпускной работы / Conference reports on the topic of the thesis

1. XII КМУ 2023, 03.04.2023 - 06.04.2023 (Конгресс, статус - всероссийский)
2. Annual Meeting Photonic Devices, 29.03.2023 - 31.03.2023 (Конференция, статус - международный)

Обучающийся/Student	Документ подписан	
	Полева Мария	

Андреевна

29.05.2023

Полева Мария Андреевна

Руководитель ВКР/
Thesis supervisor

Документ подписан

Савельев Роман Сергеевич

26.05.2023

Савельев Роман Сергеевич

CONTENTS

INTRODUCTION

For decades, the main interest of the nanophotonics community was captured by plasmonic structures due to their exceptional ability to enhance the electromagnetic fields at the subwavelength scale [1, 2, 3]. However, the significant absorption commonly observed in noble metals due to their free electron response creates many obstacles, limiting the applicability of photonic devices.

Recently, all-dielectric high-index nanoresonators have gained a lot of attention, providing tools for efficient control of the light-matter interaction [4, 5, 6]. In contrast to their plasmonic counterparts, dielectric nanoresonators exhibit minimal absorption due to the absence of free electrons. At the same time, high-index structures allow for enhancing and control of the electromagnetic fields at the nanoscale. Moreover, the quality factor of such structures is not as affected by the non-radiative losses and is mostly limited by radiative damping.

Another fascinating phenomenon which occurs in dielectric structures is their strong magnetic response, which is negligible in metallic structures because of the non-penetration of the electromagnetic field inside the metal. In accordance with the Mie theory [7, 8], both metallic and dielectric spheres can exhibit strong scattering resonances. However, the magnetic multipoles can be excited in the plasmonic structures only when the shape of the resonator is changed in order to enable the formation of the circling current inside. At the same time, the dielectric resonators of different shapes possess both magnetic and electric low-order multipole responses of the same strength, which was shown both theoretically and experimentally [9, 10, 11, 12]. Furthermore, the resonant properties of the electromagnetic response of the dielectric particles can be controlled by their shape, size and material. The condition for the excitation of the multipoles of the lowest order imposes the following limitation on the size of the nanoresonator: $d \approx \lambda/n$, where d is the characteristic size of the nanoresonator, λ is the incident wavelength so that the wavelength shrunk by the refractive index n is comparable to the particle's size.

The interference between magnetic and electric types of multipoles in the dielectric structures provides foundations for a variety of exciting effects such as zero back-scattering (Kerker effect) when amplitudes of the electric and magnetic dipoles are equal to each other. This effect could be implemented to avoid backscattering losses, which is essential for efficient waveguiding [13]. Moreover, one could derive parameters for which the front scattering is also almost zero [14,

15]. Recently, it was shown that due to the presence of both magnetic and electric dipole moments in the single constituent of the chains of the nanoresonators we can achieve unique waveguiding properties such as low transmission losses and low-loss redirection of light [16].

As was already mentioned, the Q-factors of the dielectric nanoresonators are usually bigger than that of the metallic ones, providing one of the key features of the all-dielectric structures to store the energy for a long time enhancing the near-fields [17]. However, the Q of the single dielectric resonator, which size is compared to the wavelength, predicted by the Mie theory is around 10. One could increase the quality factor of the nanoresonator by extending its sizes and achieving the excitation of whispering gallery modes [17, 18]. Moreover, providing certain conditions, one could excite supercavity modes, which for silicon resonators could have the Q of the order of 200 [19]. However, combining the dielectric resonators into different systems can result in higher numbers of the quality factor, which can find applications in sensing, lasing, and nonlinear photonics [20, 21, 22]. One way to achieve high Q-factors is by implementing the physics of the symmetry-protected bound states in the continuum (BIC) for the arrays of dielectric resonators [23, 24, 25]. The excitation of such a state is possible if the symmetry of the unitary cell of the array is broken and the state is turned into the quasi-BIC with large but finite Q [26, 27, 28]. The drawback of this approach is that all the considerations about BICs are made assuming the infinite size of the nanostructures in at least one dimension. However, in reality, we are able to work only with finite-sized systems, which impose new channels of losses lowering the values of the Q-factors [29, 30]. In this work, we will focus on a different way to achieve long storage of the energy in the systems, which basis lies in the excitation of collective modes in the finite chains of dielectric resonators of low-order Mie-modes.

An interesting example of the high-Q collective modes in the finite chains of oscillators is the band-edge mode, which frequency is the closest one to the frequency of the monotonic dispersion curve at the edge of Brillouin zone $qa \approx \pi$, where q is the Bloch wavenumber and a is the chain period, as it is shown in Fig. 1 a). Such states have been considered in photonic crystals [31], and already found their applications in lasing and sensing [30, 32, 33, 34]. The Q-factors for such modes are relatively high because in the finite chain, at such frequencies, the difference in the phases of the fields in the neighbour resonators tends to π. This

phenomenon results in destructive interference between the waves scattered by individual resonators, causing a significant reduction in radiation [35, 36]. The asymptotic behaviour of the Q-factors in the finite electric dipole chain for the band-edge modes is shown in Fig. 1b) by the blue dashed line. One can see that Q-factors of such mode are scaling as N^3 [37, 38]. It was previously shown that for the dispersion relation $\omega - \omega_0 \propto (q - q_0)^a$, the quality factor Q scales as N^{a+1} [39]. For the monotonic dispersion, only even powers contribute to the dispersion relation near the edge of the Brillouin zone, hence, $\omega - \omega_0 = c_2(q - q_0)^2 + ...$ Therefore, the third power in the Q-factor asymptotic is justified.
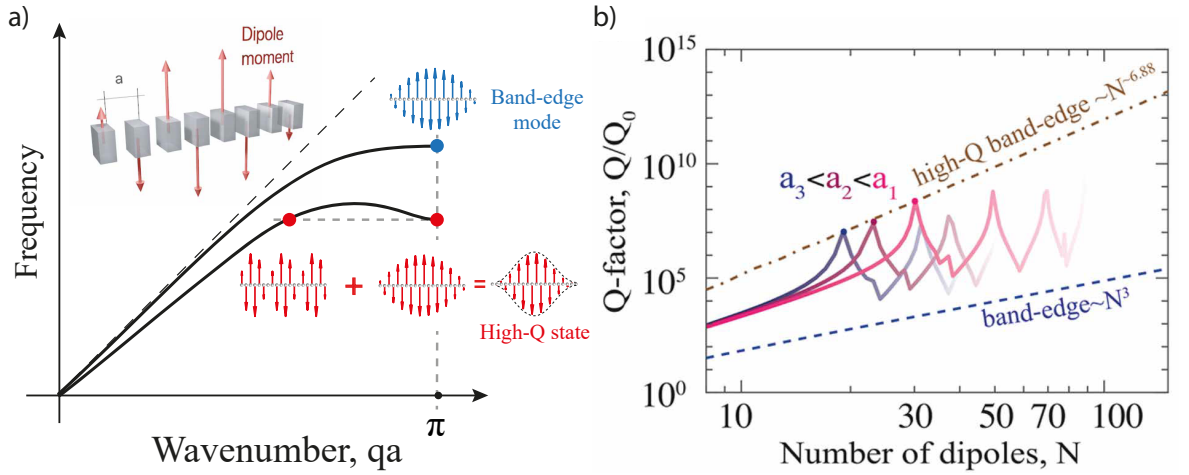

Figure 1 – a) The solution of the dispersion equation for the infinite chain of the electric dipoles representing the chain of Mie-resonant nanoparticles (insert). The inflection point on the dispersion curve triggers interference between the band-edge mode and another standing mode in a finite array. This interaction leads to the formation of a highly localized state characterized by a high-quality factor. b) The dependence of the Q-factor on the number of particles N for three different periods: $a = 0.238\lambda, 0.239\lambda, 0.240\lambda$, the maximal values for which are achieved for different numbers of particles N. The brown dashed line shows the asymptotic of the Q-factors of "high-Q" band-edge modes. The blue dashed curve corresponds to the asymptotic of the Q on N for the regular band-edge mode. The figure is reproduced from ref. [36]

The typical periods of chains of particles for which the band-edge modes can be realized are around 0.35λ [36]. However, if one starts to shrink the chain period, at some point, the dispersion will bend as it is shown in Fig. 1a). One can notice that due to the presence of the inflection point in the dispersion curve for the infinite chain, the finite chain with the same parameters supports two modes with very close frequencies, which can interact with each other constructively or

destructively via the radiation continuum. The destructive interference leads to the increase of the Q-factor of one of the two modes. The Q-factors of such "high-Q" band edge mode asymptotically scale as $N^\alpha, \alpha \approx 7$, as shown in Fig. 1b) by the brown dashed line [36]. Note that the dipoles in the considered chain are perpendicular to the axis of the chain. For the case of the dipoles oriented along the axis, the coupling constant would not have a far-field term proportional to $\propto 1/r$, and, hence, the collective interactions would be weaker, and we would not have the same effects [35].

It is important to stress that the periods of a chain of dipoles, for which the dispersion with inflection point occurs, are around 0.24λ. However, as discussed above, for the dielectric structure with Mie-type resonances, the condition for the appearance of the lowest order multipole resonances (such as a dipole resonance) is $d \approx \lambda/n$. The typical value of the refractive index in optics is around 3 [1], which means that the minimal size of the realistic dielectric nanoresonator is around 0.3λ. Moreover, the value of the period in the structures also includes the non-zero value of the gap between resonators, which makes the period of the chain of the resonant dielectric particles $a > 0.3\lambda$. However, as we saw above, for such periods in the pure electric dipole approximation, the dispersion is monotonic, and, hence, we will be able to achieve only $Q \propto N^3$. This means that we cannot predict the behaviour of the realistic resonators by using the existing model.

Using the previous discussion, we can formulate the goal of this thesis. In this work, we will construct the dipole model, with which we will be able to investigate the formation of the "high-Q" band-edge modes in the realistic chains of dielectric resonators. The model will include simultaneous electric and magnetic dipole responses of resonators, and we will analyze how the radiative losses of the chain depend on the interaction between magnetic and electric dipoles. Within this goal, we can formulate the following tasks.

In the **first chapter**, we derive the system of equations describing the infinite chain of coupled magnetic and electric dipoles both perpendicular to the axis of the chain and to each other (since only in this configuration magnetic and electric dipoles will interact with each other). We will analyze how the solutions, i.e., the dispersion branches, of such a system depend on the ratio between the resonant frequencies of magnetic and electric dipoles of a single particle. Moreover, we will compare the results with the dispersion branches of the chains of solely

magnetic or electric dipoles. Furthermore, we will approximate the electromagnetic polarizabilities, which will be embedded into the dispersion equation, with analytical functions. We will find the parameters for which one of the dispersion branches of the chain will have an inflection point. We will define the maximal values of the periods for which the bend dispersion occurs for each ratio of the frequencies. Using the obtained knowledge about the properties of the infinite chain, in the **second chapter**, we will solve the eigenproblem for the finite chains, and evaluate the dependence of the highest Q-factor from N, where N is the number of particles in the chain. We will show that, by accounting for the interaction between magnetic and electric dipoles in the chain, we can obtain the model with which it is possible to predict the radiative properties of the realistic chains of nanoresonators. To solidify our results, they will be compared with the full-wave simulations.

1 Theoretical description of the infinite chain of nanoresonators with simultaneous magnetic and electric dipolar responses

In this chapter, we describe the formation of "high-Q" band-edge modes in infinite chains of dielectric resonators with simultaneous electric and magnetic dipole responses.

1.1 Green's function

First of all, let us briefly recall Green's function formalism in order to connect the electric and magnetic fields generated by point dipole sources with their dipole moments. Note that all the following considerations are performed for the free space. To define the dyadic Green's function, we consider the electromagnetic wave equation [40, 41]:

$$\nabla \times \nabla \times \mathbf{E} - k_0^2 \mathbf{E} = i\omega\mu_0 \mathbf{j}, \tag{1}$$

where k_0 is the wave vector of the free space, ω is the corresponding wave number, μ_0 is the vacuum permeability, $\mathbf{j}$ is electric current density. The dyadic Green's tensor is a solution to the wave equation with a source distribution located at $\mathbf{r}'$:

$$\nabla \times \nabla \times \widehat{\mathbf{G}}\left(\mathbf{r}, \mathbf{r}'\right) - k_0^2 \widehat{\mathbf{G}}\left(\mathbf{r}, \mathbf{r}'\right) = i\delta\left(\mathbf{r} - \mathbf{r}'\right), \tag{2}$$

where $\widehat{\mathbf{G}}\left(\mathbf{r}, \mathbf{r}'\right)$ is the dyadic Green's tensor, $\delta\left(\mathbf{r} - \mathbf{r}'\right)$ is the delta function. Green's tensor has rank two because it connects the field vector with the current vector. The solution of equation (2) is given Green's tensor for free space:

$$\widehat{\mathbf{G}}\left(\mathbf{r}, \mathbf{r}'\right) \stackrel{\mathbf{R}=\mathbf{r}-\mathbf{r}'}{=} \widehat{\mathbf{G}}(\mathbf{R}) = \frac{e^{ik_0 R}}{4\pi R}\left[\left(1 + \frac{ik_0 R - 1}{k_0^2 R^2}\right)\widehat{\mathbf{I}} + \frac{3 - 3ik_0 R - k_0^2 R^2}{k_0^2 R^2}\frac{\mathbf{R} \otimes \mathbf{R}}{R^2}\right], \tag{3}$$

where $\widehat{\mathbf{I}}$ is 3×3 identity matrix, $\mathbf{R} \otimes \mathbf{R}$ is a tensor, which in the Cartesian coordinate system can be expressed as:

$$\mathbf{R} \otimes \mathbf{R} = \begin{pmatrix} xx & xy & xz \\ yx & yy & yz \\ zx & zy & zz \end{pmatrix}. \tag{4}$$

In the case of a point electric dipole source, the current density $\mathbf{j}$ can be expressed through the electric dipole moment $\mathbf{p}$ as:

$$\mathbf{j}(\mathbf{r}) = -i\omega\mathbf{p}\delta\left(\mathbf{r} - \mathbf{r}'\right). \tag{5}$$

Hence, the electric field of an electric dipole moment $\mathbf{p}$ is:

$$\mathbf{E}(\mathbf{r}) = \omega^2\mu_0\widehat{\mathbf{G}}\left(\mathbf{r}, \mathbf{r}'\right)\mathbf{p} = \frac{k_0^2}{\varepsilon_0}\widehat{\mathbf{G}}\left(\mathbf{r}, \mathbf{r}'\right)\mathbf{p}. \tag{6}$$

The magnetic field of the dipole moment can be found using Maxwell's equation $i\omega\mu_0\mathbf{H} = \nabla \times \mathbf{E}$:

$$\mathbf{H} = -i\omega\widehat{\mathbf{G}}^{HE}\left(\mathbf{r}, \mathbf{r}'\right)\mathbf{p} = -ikc\widehat{\mathbf{G}}^{HE}\left(\mathbf{r}, \mathbf{r}'\right)\mathbf{p}, \tag{7}$$

$$\widehat{\mathbf{G}}^{HE}\left(\mathbf{r}, \mathbf{r}'\right) = \nabla \times \widehat{\mathbf{G}}\left(\mathbf{r}, \mathbf{r}'\right) = \frac{e^{ik_0R}}{4\pi R}\frac{\left(\mathbf{R} \times \widehat{\mathbf{I}}\right)}{R^2}(ik_0R - 1), \tag{8}$$

where c is the speed of light in a vacuum, and the tensor is equal to

$$\mathbf{R} \times \widehat{\mathbf{I}} = \begin{pmatrix} 0 & -z & y \\ z & 0 & -x \\ -y & x & 0 \end{pmatrix} \tag{9}$$

Using the electromagnetic dual concept and equations (6),(7), one can also obtain electric and magnetic fields of the magnetic dipole moment $\mathbf{m}$:

$$\mathbf{E}(\mathbf{r}) = -i\frac{k}{\varepsilon_0}\widehat{\mathbf{G}}^{HE}\left(\mathbf{r}, \mathbf{r}'\right)\left(\frac{\mathbf{m}}{c}\right), \tag{10}$$

$$\mathbf{H}(\mathbf{r}) = k_0^2\widehat{\mathbf{G}}\left(\mathbf{r}, \mathbf{r}'\right)\mathbf{m}. \tag{11}$$

1.2 Equation describing eigensolutions of the chain of coupled dipoles

In this section, we will derive a dispersion equation that describes collective oscillations in chains of nanoresonators with simultaneous magnetic and electric dipolar responses.

In our case, as building blocks of the system, we consider dielectric particles, which can be represented as the composition of magnetic and electric point dipoles perpendicular to the axes of the chain. The magnetic and electric dipolar responses

of a single resonator can be represented in the following way [10, 42]:

$$\mathbf{p} = \hat{\alpha}^{\mathrm{E}} \mathbf{E}_{\mathrm{loc}} \left(\mathbf{r}' \right)$$
$$\mathbf{m} = \hat{\alpha}^{\mathrm{H}} \mathbf{H}_{\mathrm{loc}} \left(\mathbf{r}' \right),$$

(12)

$\hat{\alpha}^{\mathrm{E}}, \hat{\alpha}^{\mathrm{H}}$ are the second-rank polarizability tensors, $\mathbf{E}_{\mathrm{loc}}$ and $\mathbf{H}_{\mathrm{loc}}$ are the local electric and magnetic fields at the point of the dipole $\mathbf{r}'$. In this work, the particles that we consider possess inversion symmetry, therefore, the bianisotropic response is not taken into account, which means that magnetic and electric dipoles do not interact with each other within a single nanoresonator [43]. It is also important to note that equation (12) is written for relatively small particles neglecting non-local effects, i.e. excluding all orders of the field derivatives in the right part of (12) [42, 44].

When we consider the system consisting of a single nanoresonator then $\mathbf{E}_{\mathrm{loc}}$ and $\mathbf{H}_{\mathrm{loc}}$ are equal to the incident fields. However, if we consider the system of more than one nanoresonator it is also crucial to take into account the electric and magnetic fields created by all other particles in the system:

$$\mathbf{E}_{\mathrm{loc}} \left(\mathbf{r}' \right) = \mathbf{E}_{\mathrm{inc}} \left(\mathbf{r}' \right) + \mathbf{E}_{\mathrm{ED}} \left(\mathbf{r}' \right) + \mathbf{E}_{\mathrm{MD}} \left(\mathbf{r}' \right)$$
$$\mathbf{H}_{\mathrm{loc}} \left(\mathbf{r}' \right) = \mathbf{H}_{\mathrm{inc}} \left(\mathbf{r}' \right) + \mathbf{H}_{\mathrm{ED}} \left(\mathbf{r}' \right) + \mathbf{H}_{\mathrm{MD}} \left(\mathbf{r}' \right),$$

(13)

where $\mathbf{E}_{\mathrm{ED}}, \mathbf{E}_{\mathrm{MD}}$ are the electric fields calculated at the point of the dipole created by other electric and magnetic dipoles in the chain respectively, $\mathbf{H}_{\mathrm{ED}}, \mathbf{H}_{\mathrm{MD}}$ are the magnetic fields calculated at the point of the dipole created by other electric and magnetic dipoles. To describe the interaction between dipoles in any system suspended in a homogeneous nonmagnetic medium, one can use Green's dyadic tensor (see section 1.1), which represents the electric and magnetic fields created due to a localized source distribution in a medium, such as a dipole. This way, the electric fields produced by a chain of the magnetic and electric dipoles at the position of the j-th nanoresonator are equal to [10]:

$$\mathbf{E}_{\mathrm{ED}} \left(\mathbf{r}_j \right) = \frac{k_0^2}{\varepsilon_0} \sum_{l \neq j} \widehat{\mathbf{G}} \left(\mathbf{r}_j, \mathbf{r}_l \right) \mathbf{p}^l,$$

(14)

$$\mathbf{E}_{\mathrm{MD}} \left(\mathbf{r}_j \right) = \frac{i k_0}{c \varepsilon_0} \sum_{l \neq j} \widehat{\mathbf{G}}^{HE} \left(\mathbf{r}_j, \mathbf{r}_l \right) \mathbf{m}^l,$$

(15)

$$\mathbf{H}_{\mathrm{MD}}\left(\mathbf{r}_j\right) = k_0^2 \sum_{l \neq j} \widehat{\mathbf{G}}\left(\mathbf{r}_j, \mathbf{r}_l\right) \mathbf{m}^l, \tag{16}$$

$$\mathbf{H}_{\mathrm{ED}}\left(\mathbf{r}_j\right) = -ik_0 c \sum_{l \neq j} \widehat{\mathbf{G}}^{HE}\left(\mathbf{r}_j, \mathbf{r}_l\right) \mathbf{p}^l. \tag{17}$$

In our case, we assume the chain is oriented along the x-axis, magnetic dipoles – along the z-axis, and electric dipoles – along the y-axis as illustrated in Fig. 2.
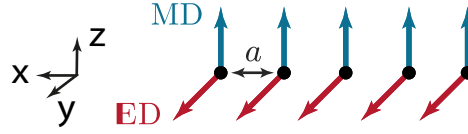

Figure 2 – Schematic depiction of the system in consideration

Therefore, the fields produced at the location of the nanoresonator at the origin:

$$E_{\mathrm{ED_y}} = \frac{k_0^2}{\varepsilon_0} \sum_{l \neq 0} G_{yy}\left(0, la\right) p^l, \tag{18}$$

$$E_{\mathrm{MD_y}} = \frac{ik_0}{c\varepsilon_0} \sum_{l \neq 0} G_{yz}^{HE}\left(0, la\right) m^l, \tag{19}$$

$$H_{\mathrm{MD_z}} = k_0^2 \sum_{l \neq 0} G_{zz}\left(0, la\right) m^l, \tag{20}$$

$$H_{\mathrm{ED_z}} = -ik_0 c \sum_{l \neq 0} G_{zy}^{HE}\left(0, la\right) p^l, \tag{21}$$

where a is the period of the chain. To calculate Green's tensor components, we first need to evaluate tensors that are incorporated into the expressions in equations (3) and (8) (see section 1.1). In (3), the tensor product is equal to:

$$\mathbf{R} \otimes \mathbf{R} = \begin{pmatrix} x^2 & 0 & 0 \\ 0 & 0 & 0 \\ 0 & 0 & 0 \end{pmatrix}. \tag{22}$$

And the tensor product in (8) is equal to

$$\mathbf{R} \times \widehat{\mathbf{I}} = \begin{pmatrix} 0 & 0 & 0 \\ 0 & 0 & -x \\ 0 & x & 0 \end{pmatrix} \qquad (23)$$

Therefore, from equation (3) in section 1.1, the components of Green's tensor connecting the electric and magnetic dipoles to the fields of the same kind are equal to

$$k_0^2 G_{yy}(0,la) = k_0^2 G_{zz}(0,la) = k_0^2 \frac{e^{ik_0 R}}{4\pi R^2} \left(1 + \frac{ik_0 R - 1}{k_0^2 R^2} \right) \stackrel{R=al}{=\!=}$$

$$\stackrel{R=dl}{=\!=} \frac{k_0^3 e^{ik_l}}{4\pi} \left(\frac{1}{k_l} + \frac{i}{k_l^2} - \frac{1}{k_l^3} \right), \qquad (24)$$

where $k_l = k_0 a |l|$. From equation (8), we can derive the expression of the Green's tensor connecting dipoles with the fields of the opposite nature:

$$k_0 G_{yz}^{HE}(0,la) = -k_0 G_{zy}^{HE}(0,la) = -k_0 \frac{e^{ik_0 R}}{4\pi R}(ik_0 R - 1)sgn(l) =$$

$$= -\frac{ik_0^3 e^{ik_l}}{4\pi} \left(\frac{1}{k_l} + \frac{i}{k_l^2} \right) sgn(l), \qquad (25)$$

where $sng(l) = \dfrac{l}{|l|}$. It is crucial to mention that in infinite systems, all dipole moments of the same nature are assumed to have the same absolute value, but different phases, which can be found using Bloch's theorem [45, 46, 47]:

$$p_l = p_0 e^{i\beta la}, \qquad (26)$$

$$m_l = m_0 e^{i\beta la} \qquad (27)$$

where p_0, m_0 are the absolute values of the magnetic and electric dipoles in the chain, β is Bloch's vector, which is defined by the properties of the system. For convenience, from this point on, we will denote $\beta_l = \beta la$.

Using the above discussion and notations, we can now rewrite the equations (12) taking into account that our aim is to solve the eigenproblem so that incident

fields are equal to zero [48, 49]:

$$\frac{p_0}{\alpha^E} = E_{\mathrm{ED_y}} + E_{\mathrm{MD_y}} = \frac{k_0^2}{\varepsilon_0} \sum_{l\neq 0} G_{yy}\left(0, la\right) p^l + \frac{ik_0}{c\varepsilon_0} \sum_{l\neq 0} G_{yz}^{HE}\left(0, la\right) m^l =$$

$$= \frac{1}{\varepsilon_0} \frac{k_0^3}{4\pi} \left[\sum_{l\neq 0} e^{ik_l} e^{i\beta_l} \left(\frac{1}{k_l} + \frac{i}{k_l^2} - \frac{1}{k_l^3} \right) p_0 + \frac{1}{c} \sum_{l\neq 0} e^{ik_l} e^{i\beta_l} \left(\frac{1}{k_l} + \frac{i}{k_l^2} \right) sgn(l) m_0 \right] =$$

$$= \frac{1}{\varepsilon_0} \left(\Sigma_1 p_0 + \frac{1}{c} \Sigma_2 m_0 \right), \text{ where}$$

(28)

$$\frac{6\pi}{k_0^3} \Sigma_1 = \frac{3}{2} \sum_{l\neq 0} e^{ik_l} e^{i\beta_l} \left(\frac{1}{k_l} + \frac{i}{k_l^2} - \frac{1}{k_l^3} \right), \quad (29)$$

$$\frac{6\pi}{k_0^3} \Sigma_2 = \frac{3}{2} \sum_{l\neq 0} e^{ik_l} e^{i\beta_l} \left(\frac{1}{k_l} + \frac{i}{k_l^2} \right) sgn(l), \quad (30)$$

One can do the same for the magnetic dipole equation:

$$\frac{m_0}{\alpha^H} = H_{\mathrm{ED_z}} + H_{\mathrm{MD_z}} = k_0^2 \sum_{l\neq 0} G_{zz}\left(0, la\right) m^l - ik_0 c \sum_{l\neq 0} G_{zy}^{HE}\left(0, la\right) p^l =$$

(31)

$$= \Sigma_1 m_0 + c \Sigma_2 p_0$$

For the sake of simplicity of expressions, in equations (28), (31) the following notation are used $\alpha^E \equiv \alpha^E_{yy}$, $\alpha^H \equiv \alpha^H_{zz}$. With all the necessary ingredients, we can now compose the system of equations, which describes the properties of the chain of nanoresonators with both electric and magnetic dipole responses:

$$\begin{cases} (p_0 c)\left(\dfrac{\varepsilon_0}{\alpha^E} - \Sigma_1 \right) - \Sigma_2 m_0 = 0 \\[2mm] m_0 \left(\dfrac{1}{\alpha^H} - \Sigma_1 \right) - \Sigma_2 (p_0 c) = 0. \end{cases}$$

(32)

From the Rouché–Capelli theorem we know, that in order for this system to have a nontrivial solution, the determinant of the matrix representing this system should be equal to zero:

$$\begin{vmatrix} \left(\dfrac{\varepsilon_0}{\alpha_E} - \Sigma_1 \right) & -\Sigma_2 \\[2mm] -\Sigma_2 & \left(\dfrac{1}{\alpha_H} - \Sigma_1 \right) \end{vmatrix} = 0, \quad (33)$$

which means that the dispersion of the infinite chain is as follows:

$$\left(\frac{1}{\alpha_m} - \Sigma_1\right) \cdot \left(\frac{\varepsilon_0}{\alpha_e} - \Sigma_1\right) - \Sigma_2^2 = 0. \tag{34}$$

For convenience, we rewrite our equation:

$$\left(\frac{6\pi}{k_0^3}\frac{1}{\alpha_m} - \frac{6\pi}{k_0^3}\Sigma_1\right) \cdot \left(\frac{6\pi}{k_0^3}\frac{\varepsilon_0}{\alpha_e} - \frac{6\pi}{k_0^3}\Sigma_1\right) - \left(\frac{6\pi}{k_0^3}\right)^2 \Sigma_2^2 = 0. \tag{35}$$

In equation (35), we now have the expressions from equations (29), (30), which were calculated before [48, 49]. The imaginary part of the dipole sum is $\mathrm{Im}\left(\frac{6\pi}{k_0^3}\Sigma_1\right) = -i$, while the real part reads as follows:

$$\widetilde{\Sigma_1} = -\mathrm{Re}\left(\frac{6\pi}{k_0^3}\Sigma_1\right) = -3\mathrm{Re}\left(\sum_{j=1}^{\infty} e^{ik_j}\cos(\beta_j)\left(\frac{1}{k_j} + \frac{i}{k_j^2} - \frac{1}{k_j^3}\right)\right) =$$

$$= \frac{3}{2}\sum_{j=1}^{\infty}\left(\frac{\cos(\beta_j + k_j) + \cos(\beta_j - k_j)}{k_j^3} + \frac{\sin(\beta_j + k_j) - \sin(\beta_j - k_j)}{k_j^2}\right) \tag{36}$$

$$+ \frac{3}{2}\frac{\ln[2(\cos(k_0 a) - \cos(\beta a))]}{k_0 a}.$$

Let us also assign a new variable to the dispersion equation component containing (30), which represents the coupling between electric and magnetic dipoles in the chain, in the same way, that is done for Σ_1. Note that the imaginary part of the Σ_2 is zero, and the real part is [48]:

$$\widetilde{\Sigma_2} = \mathrm{Re}\left(\frac{6\pi}{k_0^3}\Sigma_2\right) = -\frac{3}{2}\sum_{j=1}^{\infty}\left(\frac{\sin(\beta_j + k_j) + \sin(\beta_j - k_j)}{k_j^2}\right) -$$

$$- \frac{3}{2}\frac{1}{k_0 a}\left(\ln\left|\frac{\sin(\beta a + k_0 a)}{2}\right| - \ln\left|\frac{\sin(\beta a - k_0 a)}{2}\right|\right). \tag{37}$$

Note that since dipole sums Σ_1 and Σ_2 depend on the wave number k_0, they are functions of frequency $\Sigma_1 = \Sigma_1(\omega), \Sigma_2 = \Sigma_2(\omega)$. Now, to solve the equation (35) and find eigenfrequencies of the chain of nanoparticles with magnetic and electric dipole responses, we need to define the frequency dependence of the polarizabilities α^E and α^H.

1.3 Magnetic and electric polarizabilities

In this section, the choice of the functions representing electromagnetic polarizabilities α^E and α^H will be discussed.

Obviously, the most straightforward way to obtain the dependence of polarizabilities on frequency is to extract them from numerical full-wave simulations. In the following sections, we will compare the results of the dipole model to the full-wave simulation for cylindrical nanoparticles, which makes the following example relevant. For instance, one can consider plane-wave irradiation of a particle of interest in COMSOL Multiphysics. In Fig. 3, one can find the multipolar decomposition of the scattering cross section of the dielectric cylinder under irradiation of a plane wave incident along the z-axis with the polarization of the electric field along the x-axis. Multipole moments of the cylinder along with their contributions to the scattering cross section are calculated using formulas from [11, 50, 51]. It is important to choose the spectral range where the nanoresonator has only magnetic and electric dipolar responses. One can see that at the values of angular frequency in the interval $\approx [3.8 \cdot 10^{10}, 6.5 \cdot 10^{10}]$ rad/s, only electric and magnetic dipoles contribute to the total scattering cross-section, since the sum of their contributions in this range is equal to the total cross-section. This also means that there are no higher-order multipoles contributing to the scattering for the considered spectral range. Thus, this frequency range is suitable for the model that we are building. The dipole polarizabilities can be extracted from the complex values of the dipoles also calculated in COMSOL by dividing the dipole moments on the corresponding incident fields (see equation (12)) [50].

However, one might take a more analytical approach to define the polarizabilities so that our model will be more general and applicable to different geometries and sizes of the particles forming the chain. We want to be able to solve the dispersion equation for the particles with different resonant properties, which means that we need to incorporate the resonant frequencies into the polarizabilities as parameters. Let us first consider the electromagnetic response of the spherical nanoparticle on the incident plane wave. The polarization and direction of incidence are irrelevant for our purposes. The exact solution of Maxwell's equation for the sphere is well known from Mie theory [7, 8] and is presented in Fig.4. In this picture, we observe two first dipole resonances in the range, where other higher-order multipoles are negligible. One can notice that compared to the case
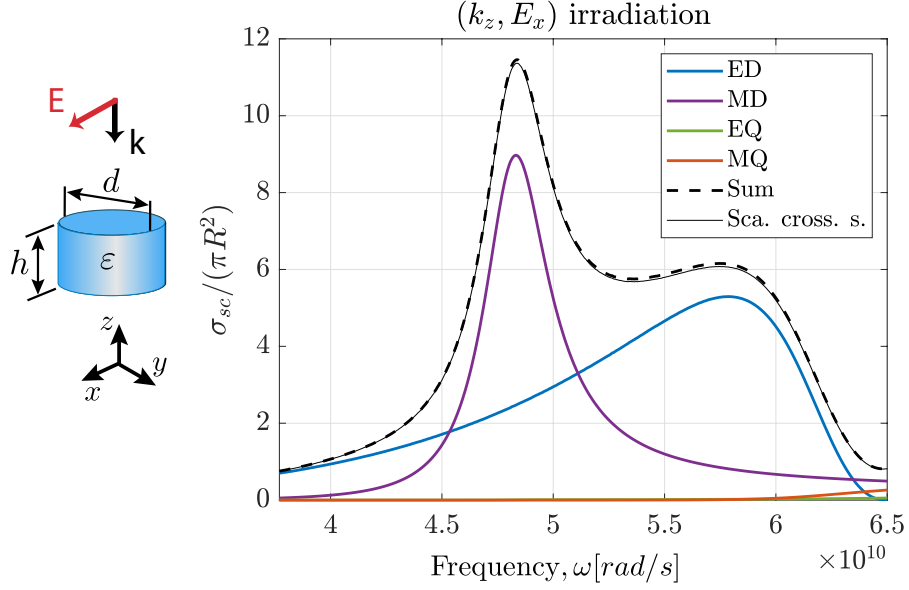
Figure 3 – Normalized scattering cross-section $\sigma_{sc}/(\pi R^2)$ and its multipole decomposition into electric dipole (ED), magnetic dipole (MD), electric quadrupole (EQ), and magnetic quadrupole (MQ) terms normalized on the surface of the base of the cylinder-shaped nanoparticle. The incident plane wave is x-polarized and propagates along the z-axis. The parameters of the cylinder: diameter of the base of the cylinder $d = 10$ mm, the height of the cylinder $h = 7$ mm, the relative permittivity of the material $\varepsilon = 15.4$

of the cylinder in Fig. 3, the sphere has pronounced magnetic quadrupole resonance in the vicinity of the "dipole range". However, we will not account for this resonance in our further considerations, and later it will be shown that the model still works well and results are in agreement with full-wave simulations. Note that electromagnetic polarizabilities of a sphere are known from Mie theory as a function of the scattering Mie coefficients with a quite complicated dependence on the frequency [26]. However, since our aim is to construct a function of frequency, which may also help to describe the polarizabilities of different shapes of nanoparticles, we will not use this expression. Instead of this, we construct the analytical polarizabilities with simpler dependence on the frequency.

1.3.1 Analytical expression for magnetic polarizability

In this section, we will derive the expression for the magnetic polarizability, and more specifically for the reversed polarizability $1/\alpha^H$. From Fig.4, one can see that the real magnetic dipole contribution near resonance can be fitted with a
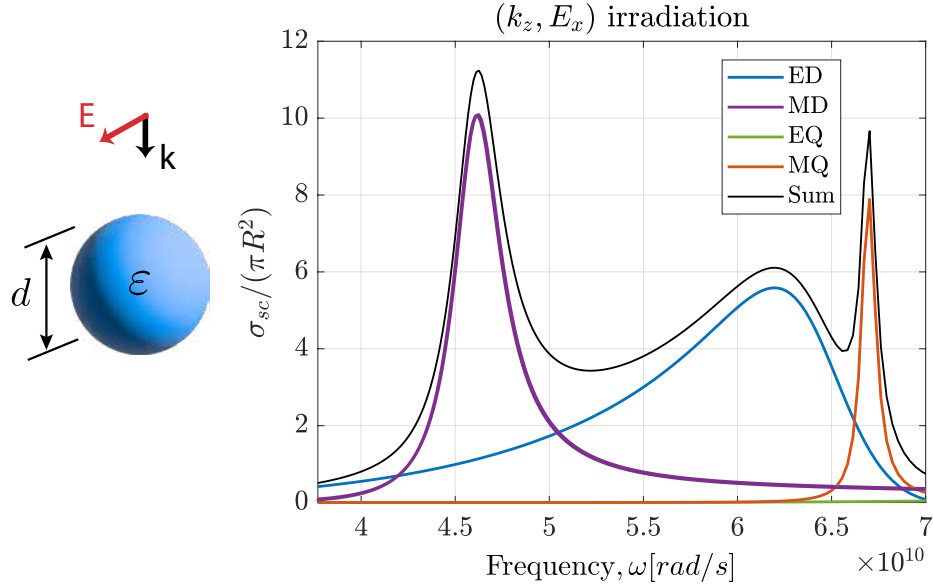
Figure 4 – Normalized scattering cross-section $\sigma_{sc}/(\pi R^2)$ and its multipole decomposition into electric dipole (ED), magnetic dipole (MD), electric quadrupole (EQ), and magnetic quadrupole (MQ) terms for the spherical nanoparticle. The parameters of the sphere: diameter $d = 10$ mm, relative permittivity of the material $\varepsilon = 15.4$

Lorentzian function of the following form:

$$\frac{1}{\alpha_{(r)}^H} = \frac{\omega_m - i\gamma_m - \omega}{\Gamma_m}, \tag{38}$$

where α_r^H is the dipole polarizability near magnetic dipole resonance, $\frac{\gamma_m}{\Gamma_m} = \frac{k_0^3}{6\pi}$ so that the imaginary part of the reversed polarizability is defined solely by the radiative losses [50], γ_m is defined via the half width at the half maximum of the magnetic resonance, and ω_m is the resonant frequency of magnetic dipole. All the parameters can be derived from fitting the magnetic dipole cross-section with the Lorentzian profile or from the eigenmodes calculation in COMSOL Multiphysics, $\gamma_m = \omega_m/2/Q_m$, where Q_m is the quality factor of this mode. The calculated parameters are as follows: $\omega_m \approx 4.8 \cdot 10^{10}$ rad/s, $Q_m = 13.2$.

Now, we can compare the approximated analytical expression for polarizability with the magnetic dipole contribution to the cross-section from Mie theory in Fig. 4 using the following expression [50]:

$$\sigma_{\text{sca}} \simeq \frac{k_0^4}{6\pi\varepsilon_0^2 |\mathbf{E}_{\text{inc}}|^2} |\mathbf{p}|^2 + \frac{k_0^4 \mu_0}{6\pi\varepsilon_0 |\mathbf{E}_{\text{inc}}|^2} |\mathbf{m}|^2 = \frac{k_0^4}{6\pi} \left|\frac{\alpha^E}{\varepsilon_0}\right|^2 + \frac{k_0^4}{6\pi}|\alpha^H|^2, \tag{39}$$

where we used equation (12), and the fact that for the free space, the relation between magnetic and electric fields is equal to the wave impedance $\frac{E}{H} = Z_0 = \sqrt{\frac{\mu_0}{\varepsilon_0}}$. The results of the comparison are presented in Fig. 5(a). One can see that the approximation for α_r^H works well close to the magnetic dipole resonance. However, at frequencies slightly below and above the resonance, the difference between the approximation and Mie theory becomes non-negligible. Note that this difference with an exact solution can become crucial when we solve the dispersion equation (34) near the light line. To overcome the disagreement with the theory, one can introduce the power factor $(\omega_m/\omega)^n$ to the real part of the polarizabilities. For the frequencies $\omega > \omega_m$ this factor will decrease the approximated values of the cross-section, and increase for the frequencies $\omega < \omega_m$, and at the same time would not affect the region near resonance much. The power n can differ for different geometries. For instance, for the sphere n should be equal to 4, as can be seen from Fig. 5(b) and Fig. 5(c). The final expression for the approximated reversed magnetic polarizability is as follows:

$$\frac{1}{\alpha^H} = \frac{\omega_m - \omega}{\Gamma_m} \frac{\omega_m^n}{\omega^n} - i\frac{\gamma_m}{\Gamma_m} = \frac{\omega_m - \omega}{\gamma_m} \frac{k_0^3}{6\pi} \frac{\omega_m^n}{\omega^n} - i\frac{k_0^3}{6\pi}. \tag{40}$$
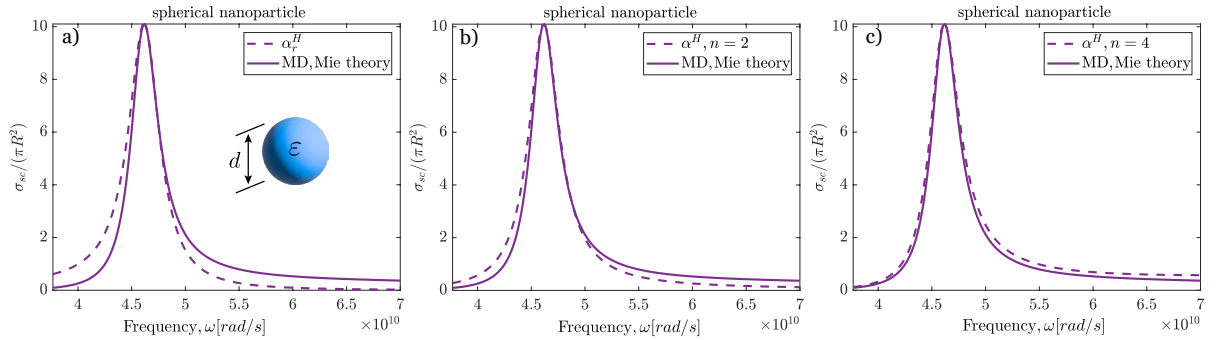

Figure 5 – Comparison of the normalized scattering cross-section $\sigma_{sc}/(\pi R^2)$ of the magnetic dipole of the sphere calculated using Mie theory and a) Lorentz approximation of the curve, b) Lorentz approximation corrected by the factor $(\omega_m/\omega)^n, n = 2$, c) Lorentz approximation corrected by the factor $(\omega_m/\omega)^n, n = 4$. The parameters of the sphere are: diameter $d = 10$ mm, relative permittivity of the material $\varepsilon = 15.4$

One can also compare the cross-section using the analytical form of α^H and COMSOL Multiphysics for a cylindrical nanoparticle. Parameters for the approximation of the magnetic dipole resonance of a cylinder can be also extracted from

the eigensolver in COMSOL, and are as follows, $\omega_m \approx 4.84 \cdot 10^{10}$ rad/s, $Q_m = 13$. The results of the approximation for n equal to 2,3, and 4 are presented in Fig.6(a), Fig.6(b), Fig.6(c). One can notice that for all three of the cases, the resonances of the numerically calculated dipole moment and approximated one does not exactly coincide. This is because the solution extracted from COMSOL is an approximated one. In this particular case, the resonant is quite narrow, so the step of the calculation was not small enough and the preciseness of the mesh was not good enough. These problems with finding the numerical solution with the appropriate level of preciseness are the reason why we choose the spherical nanoparticle for the search of the approximated analytical expressions of α. Nevertheless, we can conclude that the model of the magnetic polarizability presented in equation (40) works well for the cylinder-shaped nanoparticles. Moreover, the most suitable power of the correctional factor n is also equal to 4.

Despite the fact that, for both spherical and cylindrical nanoresonators, the most suitable $n = 4$, later on, it will be shown that in some cases $n = 2$ is better suited.
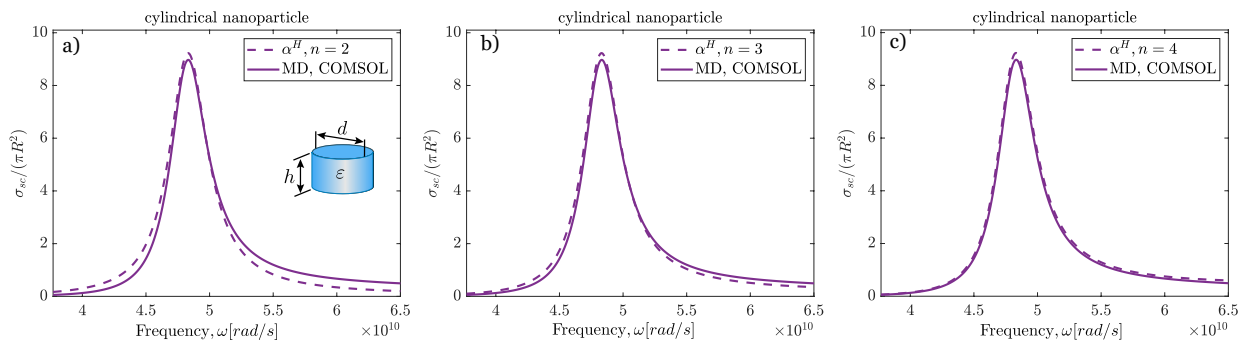

Figure 6 – Comparison of the normalized scattering cross-section $\sigma_{sc}/(\pi R^2)$ of the magnetic dipole of the sphere calculated using COMSOL Multiphysics and Lorentz approximation corrected by the factor $(\omega_m/\omega)^n$, a) $n = 2$, b) $n = 3$, c) $n = 4$. The parameters of the cylinder are: diameter of the cylinder base $d = 10$ mm, the cylinder height $h = 7$ mm, the relative permittivity of the material
$$\varepsilon = 15.4$$

1.3.2 Analytical expression for electric polarizability

As soon as we try to approximate the electric dipole polarizability α^E, we can notice that the Lorentzian would not fit the form of the electric dipole contribution to the cross-section. As it can be seen from Fig. 4, the shape of the curve resembles the Fano resonance profile. It is easier to define the reversed electric dipole polarizability since the pole of its real part correspond to zero of the elec-

tric dipole contribution to the total cross-section, while zero of the real part of the reversed polarizability indicates the local maximum of the cross-section [52]. One can assume that the real part of the reversed electric polarizability is as follows:

$$Re\left(\frac{\varepsilon_0}{\alpha^E}\right) = \frac{G}{F},\tag{41}$$

where G, F are the functions of frequency. Then, using the knowledge that at the resonant frequency the reversed polarizability should be equal to zero, we understand that the function G should be proportional to $(\omega_e - \omega)$, where ω_e is the electric dipole resonant frequency. When the value of the electric dipole cross-section reaches zero instead, the reversed polarizability should gravitate towards infinity in this region. Thus, it makes sense to assume that the function F should be proportional to $(\omega_{e2} - \omega)$, where ω_{e2} is the frequency at which the electric dipole scattering turns zero. Another important point is that in the region of small frequencies, the electric dipole polarizability should become equal to the electrostatic polarizability [8]:

$$\frac{1}{\alpha_0} = \frac{\varepsilon + 2}{3V(\varepsilon - 1)},\tag{42}$$

where V is the volume of a sphere, and ε is its relative permittivity. Hence, the final expression for electric polarizability, including the imaginary part, which is again determined by dipole radiative losses, is:

$$\frac{\varepsilon_0}{\alpha^E} = \frac{1}{\alpha_0}\frac{1 - \omega/\omega_e}{1 - \omega/\omega_{e2}} - i\frac{k_0^3}{6\pi},\tag{43}$$

One can notice that for small frequencies, both ω/ω_e and ω/ω_{e2} go to zero, and the real part of the electric polarizability indeed becomes equal to the electrostatic one. For convenience, let us modify the expression in the equation 43:

$$\frac{\varepsilon_0}{\alpha^E} = C_0\frac{1 - \omega/\omega_e}{1 - \omega/\omega_{e2}}\frac{k_0^3}{6\pi} - i\frac{k_0^3}{6\pi},\tag{44}$$

where $C_0 = \dfrac{2\pi(\varepsilon + 2)}{(\varepsilon - 1)k_0^3 V}$.

Let us now compare the results of the electric dipole cross-section calculated with the approximated electric polarizability (44) using equation (39) and the exact solution for the spherical nanoparticle. The parameters necessary for the

approximation and extracted from the Mie theory are as follows: $\omega_e = 6.2$ rad/s, $\omega_{e2} = 7.1$ rad/s. The results of the comparison are presented in Fig. 7a). One can see that for a spherical nanoparticle, the model works almost perfectly. However, for a cylindrical nanoresonator, the cross-section calculated within the built model differs from the one calculated in COMSOL as it is shown in Fig.7b). The parameters of the cylinder extracted from COMSOL Multiphysics are as follows: $\omega_e = 5.8$ rad/s, $\omega_{e2} = 6.4$ rad/s. However, we will still use this model, later on, to describe the polarizability of a cylinder in the chain, and the results will still show good agreement with full-wave simulations. Note the values of the approximated dipole cross-section for the sphere and cylinder differ from each other since electrostatic polarizability α_0 contains the volume of the nanoresonator V, which is not the same in these two cases.

It is important to understand that the derived rough approximations of polarizabilities while not being comprehensive, can still highlight the primary factors that influence the overall behaviour of the dispersion of the chain that will be considered below.
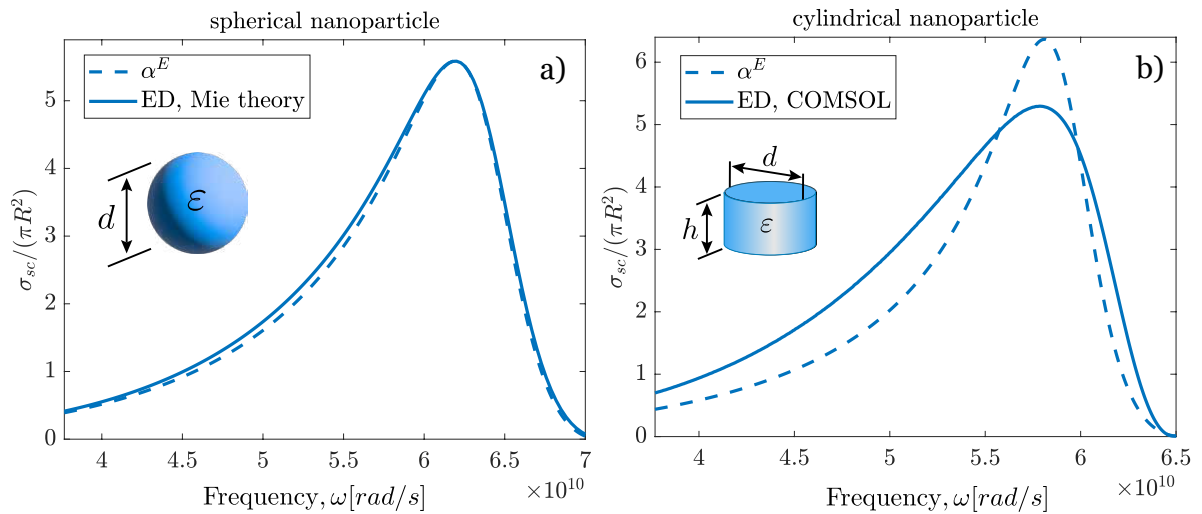

Figure 7 – Comparison of the normalized scattering cross-section $\sigma_{sc}/(\pi R^2)$ calculated with the approximated value of the electric polarizability (43) with the cross-section of the electric dipole of the a) spherical nanoparticle calculated using Mie's theory, and b) cylindrical nanoparticle calculated using COMSOL Multiphysics. The parameters of the sphere in a) are: diameter $d = 10$ mm, the relative permittivity of the material $\varepsilon = 15.4$. The parameters of the cylinder in b) are: diameter of the cylinder base $d = 10$ mm, the cylinder height $h = 7$ mm, the relative permittivity of the material $\varepsilon = 15.4$

1.4 Chain of magnetic dipoles

In this section, we will solve the dispersion equation for the chain of the solely magnetic dipolar resonators with magnetic polarizability introduced in section 1.3. This step is essential for analyzing the behaviour of the chain with two types of resonances. Note that the dipole model itself, in our case, is the set of equations representing the chain of interacting dipoles. This means that the shape of the nanoresonators, which properties are represented by the polarizabilities of a single nanoresonator α^H or α^E, does not matter. Especially considering the fact that the analytical function for the polarizability α^H introduced in equation (40) does not directly depend on the shape of the nanoresonator, but only on its resonant properties.

From equation (34), excluding all the parts related to the electric dipoles, we obtain the following equation:

$$\left(\frac{1}{\alpha_H} - \Sigma_1 \right) = 0. \tag{45}$$

Hence, using the obtained approximation for the magnetic polarizability (40), we get the following equation:

$$\frac{\omega_m - \omega}{\gamma_m} \frac{k_0^3}{6\pi} \frac{\omega_m^n}{\omega^n} - i\frac{k_0^3}{6\pi} - \Sigma_1 = 0, \tag{46}$$

If we now multiply both parts by $\gamma_m \dfrac{6\pi}{k_0^3} \dfrac{\omega^n}{\omega_m^n}$, we will obtain:

$$(\omega_m - \omega) - i\gamma_m \frac{\omega^n}{\omega_m^n} - \gamma_m \frac{\omega^n}{\omega_m^n} \frac{6\pi}{k_0^3} \Sigma_1 = 0. \tag{47}$$

As mentioned before, $\dfrac{6\pi}{k_0^3}\Sigma_1 = -i$. Hence:

$$\omega = \omega_m - \frac{\omega^n}{\omega_m^n}\gamma_m \mathrm{Re}\left(\frac{6\pi}{k_0^3}\Sigma_1 \right). \tag{48}$$

Since Σ_1 is a function of frequency, the equation in (48) is transcendental. Using that $\mathrm{Re}\left(\dfrac{6\pi}{k_0^3}\Sigma_1 \right) = -\widetilde{\Sigma_1}$ [see equation (36)], we obtain the eigenproblem for the

chain of magnetic dipole resonators:

$$\omega_{MD} = \omega_m + \frac{\omega^n}{\omega_m^n}\gamma_m\widetilde{\Sigma_1}. \tag{49}$$

The obtained equation is solved numerically in MATLAB using the $fzero$ function. The results of the simulation are presented in Fig. 8. One can notice that for the normalized periods a/λ_m approaching 0.3, the dispersion becomes monotonic. Here λ_m is the wavelength of the magnetic dipole resonance of the single nanoresonator. However, for periods around $a/\lambda_m \approx 0.2$ and lower, the dispersion has an inflection point. The presence of the inflection point in the dispersion results in a huge increase of the Q-factors in the finite chains with the same parameters as in the infinite chain as will be shown later for the simulations for the finite chains. One can also calculate numerically the maximal period a_{crit}, for which dispersion is still nonmonotonic. For the chain of the nanoresonators with pure magnetic dipole response, $a_{\text{crit}} \approx 0.24 \cdot \lambda_m$.
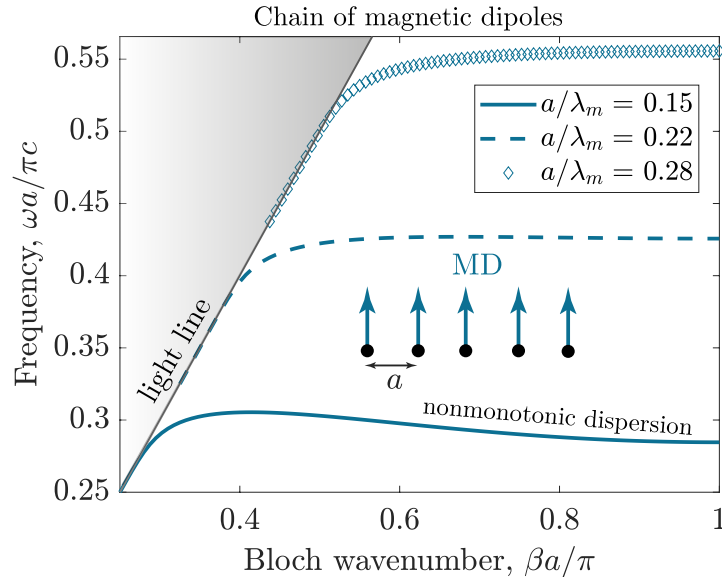

Figure 8 – Solution of dispersion equation (49) for the chain of interacting magnetic dipoles with different periods of the chain $a = 6, 8.5, 11$ mm normalized on the wavelength of the magnetic dipole resonance of a single resonator $\lambda_m \approx 39.2$ mm. The parameters of the cylindrical resonator are incorporated into the dipole model. The horizontal axis corresponds to the Bloch-vector multiplied by the factor a/π, and the vertical axis corresponds to the frequency ω multiplied by the factor $a/\pi c$

1.5 Chain of electric dipoles

In this section, we will solve the dispersion equation for the chain of the solely electric dipolar resonators with the electric polarizability (43). We emphasize again that the shape of the nanoresonators does not matter when considering the dipole model since the only component of the dispersion equation, in which the properties of the nanoresonator are encoded, is the polarizability α. However, one might notice that, in terms of our model, polarizabilities in equations (43), (40), the only difference for different geometries is the volume V of the nanoresonator, incorporated into the expressions for α^E.

From equation (34), excluding all the parts related to the magnetic dipoles, we obtain the following equation:

$$\left(\frac{\varepsilon_0}{\alpha^E} - \Sigma_1 \right) = 0. \tag{50}$$

using the expression for the electric polarizability α^E in equation (44), we get the equation in the following form:

$$C_0 \frac{1 - \omega/\omega_e}{1 - \omega/\omega_{e2}} \frac{k_0^3}{6\pi} - i \frac{k_0^3}{6\pi} - \Sigma_1 = 0. \tag{51}$$

As mentioned before, $\mathrm{Im}\left(\frac{6\pi}{k_0^3} \Sigma_1 \right) = -i$, and $\mathrm{Re}\left(\frac{6\pi}{k_0^3} \Sigma_1 \right) = -\widetilde{\Sigma_1}$ (equation (36)), thus:

$$C_0 \frac{1 - \omega/\omega_e}{1 - \omega/\omega_{e2}} + \widetilde{\Sigma_1} = 0. \tag{52}$$

We can now transform this equation to a more convenient form:

$$C_0(1 - \omega/\omega_e) + \widetilde{\Sigma_1}(1 - \omega/\omega_{e2}) = 0, \tag{53}$$

$$C_0 + \Sigma_1 = \omega \left(\frac{C_0}{\omega_e} + \frac{\Sigma_1}{\omega_{e2}} \right). \tag{54}$$

After that, we obtain the eigenproblem for the chain of electric dipole resonators:

$$\omega_{ED} = \frac{C_0 + \widetilde{\Sigma_1}}{C_0/\omega_e + \widetilde{\Sigma_1}/\omega_{e2}}. \tag{55}$$

The obtained equation can now be solved numerically with the help of MATLAB. The results of the simulations are presented in Fig. 9. One can notice that for the normalized periods a/λ_e, where λ_e is the resonant wavelength of the electric dipole resonance of the single constituent of the chain, approaching $0.3\lambda_e$, the dispersion becomes monotonic. However, for periods around $0.2\lambda_e$ and lower, the dispersion has an inflection point. Using numerical methods, one can calculate the maximal period a_{crit}, for which dispersion is still nonmonotonic. For the chain of the nanoresonators with single electric dipole response, $a_{\text{crit}} \approx 0.24 \cdot \lambda_e$, which is the same as the magnetic dipoles chain maximal period with nonmonotonic dispersion.
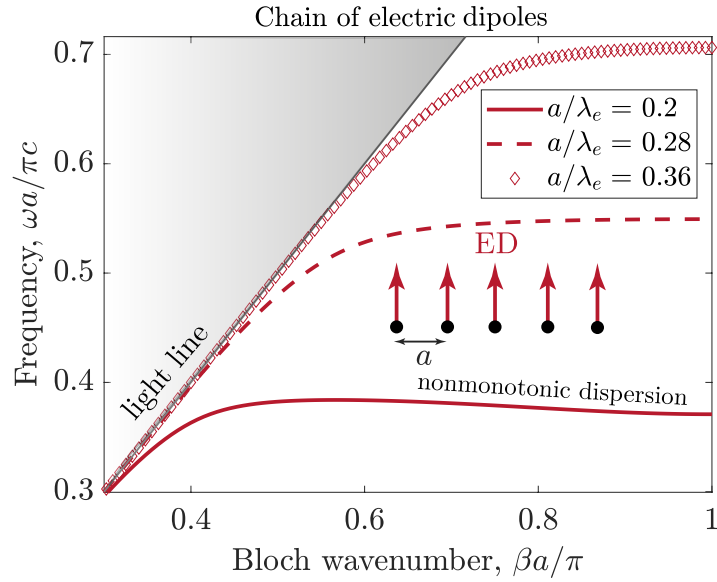

Figure 9 – Solution of the eigenproblem in equation (50) in the dipole model of the chain of interacting electric dipoles for different periods of the chain $a = 6, 8.5, 11$ mm normalized on the resonant wavelength of the magnetic dipole $\lambda_e \approx 30.4$ mm for the single resonator, parameters of which are incorporated into the dipole model. The horizontal axis corresponds to the Bloch-vector multiplied by the factor a/π, and the vertical axis corresponds to the frequency ω multiplied by the factor $a/\pi c$

1.6 Chain of coupled electric and magnetic dipoles

In this section, we will analyze the behavior of the chain of the coupled magnetic and electric dipoles, and compare the results with results for the single dipole models discussed in previous sections. The equation on eigenfrequencies

for this problem was derived in section 1.2:

$$\left(\frac{6\pi}{k_0^3} \frac{1}{\alpha^H} - \frac{6\pi}{k_0^3} \Sigma_1 \right) \cdot \left(\frac{6\pi}{k_0^3} \frac{\varepsilon_0}{\alpha^E} - \frac{6\pi}{k_0^3} \Sigma_1 \right) - \left(\frac{6\pi}{k_0^3} \right)^2 \Sigma_2^2 = 0.$$

We can rewrite this equation using equation (48) and equation (52):

$$\left((\omega_m - \omega) \frac{\omega_m^n}{\omega^n} + \gamma_m \widetilde{\Sigma_1} \right) \left(C_0 \frac{1 - \omega/\omega_e}{1 - \omega/\omega_{e2}} + \widetilde{\Sigma_1} \right) - \gamma_m \widetilde{\Sigma_2}^2 = 0. \qquad (56)$$

If we multiply this equation by $\dfrac{\omega^n}{\omega_m^n} \cdot (1 - \omega/\omega_{e2})$, we will receive:

$$\left((\omega_m - \omega) + \gamma_m \widetilde{\Sigma_1} \frac{\omega^n}{\omega_m^n} \right) \left(C_0 (1 - \omega/\omega_e) + \widetilde{\Sigma_1} (1 - \omega/\omega_{e2}) \right) - $$
$$- \frac{\omega^n}{\omega_m^n} (1 - \omega/\omega_{e2}) \gamma_m \widetilde{\Sigma_2}^2 = 0. \qquad (57)$$

We can simplify this expression using equation (49) and further altering the right bracket:

$$(-\omega + \omega_{MD}) \left(\left(C_0 + \widetilde{\Sigma_1} \right) - \omega \left(C_0/\omega_e + \widetilde{\Sigma_1}/\omega_{e2} \right) \right) - $$
$$- \frac{\omega^n}{\omega_m^n} (1 - \omega/\omega_{e2}) \gamma_m \widetilde{\Sigma_2}^2 = 0. \qquad (58)$$

The last step is to divide everything by $\left(C_0/\omega_e + \widetilde{\Sigma_1}/\omega_{e2} \right)$:

$$(-\omega + \omega_{MD}) \left(\frac{C_0 + \widetilde{\Sigma_1}}{C_0/\omega_e + \widetilde{\Sigma_1}/\omega_{e2}} - \omega \right) - \frac{\omega^n}{\omega_m^n} \frac{1 - \omega/\omega_{e2}}{C_0/\omega_e + \widetilde{\Sigma_1}/\omega_{e2}} \gamma_m \widetilde{\Sigma_2}^2 = 0. \quad (59)$$

Using the equation (55), we finalize the dispersion equation for the chain of coupled dipoles:

$$(\omega - \omega_{MD})(\omega - \omega_{ED}) + \frac{C_e}{\omega_{e2}} \omega - C_e = 0, \qquad (60)$$

where $C_e = \dfrac{\gamma_m \widetilde{\Sigma_2}^2}{C_0/\omega_e + \widetilde{\Sigma_1}/\omega_{e2}} \dfrac{\omega^n}{\omega_m^n}$.

From the last equation, we see that all the coupling effects are embedded into C_e. While resembling the quadratic equation, the eigenproblem in (60) has a more complicated dependence on frequency due to the fact that dipole sums $\widetilde{\Sigma_1}$

and $\widetilde{\Sigma_2}$ also depend on frequency. However, this equation still has 2 solutions, which we obtain using MATLAB. We will show the results for $n = 2$ and $n = 4$ in the magnetic polarizability α^H in equation (40). Parameters of the simulation are $\omega_m = 4.8 \cdot 10^{10}$ rad/s, $\omega_e = 5.8 \cdot 10^{10}$ rad/s, $Q_m = 13$, $\omega_{e2} = 6.4 \cdot 10^{10}$ rad/s, $a = 10.3$ mm (the period of the chain), the relative permittivity of the resonator, which properties are incorporated into polarizabilities $\varepsilon = 15.4$, the volume $V \approx 549$ mm^3. The results of the simulations are presented in Fig. 10. In this picture, 2 solutions of the equation (60) are presented, as well as the solutions for the single dipole chains. The eigenvalues of the chain of coupled dipoles are coloured according to the values of the ratio $|pc/m|$ for each value of the Bloch wave vector. The ratio was calculated using the first equation in the system (32):

$$(pc) \left(\frac{6\pi\varepsilon_0}{k_0^3 \alpha^E} - \frac{6\pi}{k_0^3} \Sigma_1 \right) - \frac{6\pi}{k_0^3} \Sigma_2 m = 0. \tag{61}$$

From this, using equation (43), we can obtain the relation between magnetic and electric dipoles for the dispersion solution:

$$\left| \frac{pc}{m} \right| = \left| \frac{\frac{6\pi\varepsilon_0}{k_0^3} \text{Re} \left[\frac{1}{\alpha^E} \right] + \widetilde{\Sigma_1}}{\widetilde{\Sigma_2}} \right|. \tag{62}$$

Note that this relation is calculated after obtaining the eigenfrequencies by substituting them into the dipole sums $\widetilde{\Sigma_1}, \widetilde{\Sigma_2}$ and the polarizability α^E. It is also important to mention that frequencies along the y-axis in Fig. 10 are normalized differently compared to the previous sections. For illustrative purposes, we normalize all the y-axis values by ω_e to make a visual distinction between "ED modes" and "MD modes". One can notice that the upper branch of the coupled chain eigenfrequencies is close to 1 when approaching the edge of the Brillouin zone, which is the indicator that this mode belongs to the "ED modes". Moreover, it can be seen that the $log_{10} \left| \frac{pc}{m} \right|$ ratio for this branch is indicated by the red colour, meaning that the electric dipole is the main contributing dipole to the eigenvector corresponding to this mode. In contrast, the lower branch solution of the dispersion equation is mostly blue, indicating that this the ratio $log_{10} \left| \frac{pc}{m} \right|$ is small, so this mode corresponds to the "MD modes".
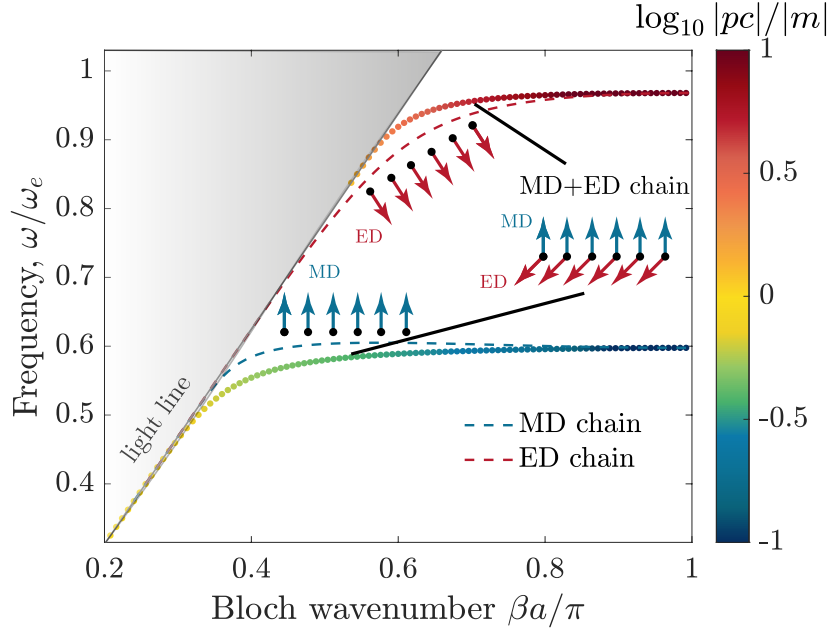
Figure 10 – Solution of the dispersion equation (60) in the dipole model for the chain of coupled magnetic and electric dipoles. The period of the chain is $a/\lambda_e = 0.32$ normalized by the resonant wavelength of the electric dipole $\lambda_e \approx 30.4$ mm for the single resonator, parameters of which are incorporated into the dipole model. The horizontal axis corresponds to the Bloch wave number multiplied by the factor a/π, and the vertical axis corresponds to the frequency ω divided by the resonant frequency of the electric dipole of a single resonator ω_e. The colorbar represents the ratio $|pc/m|$ of the eigenvectors for two coupled dipole branches. The blue dashed line corresponds to the solution of the eigenproblem given by equation (49) in the dipole model for the chain of interacting magnetic dipoles, the red one – to the solution of the eigenproblem given by equation (50) in the dipole model of the chain of interacting electric dipoles. The gray area corresponds to the states above the light line. Parameters of the simulation are $\omega_m = 4.8 \cdot 10^{10}$ rad/s, $\omega_e = 5.8 \cdot 10^{10}$ rad/s, $Q_m = 13$, $\omega_{e2} = 6.4 \cdot 10^{10}$ rad/s, $a = 10.3$ mm (the period of the chain), the relative permittivity of the resonator, which properties are incorporated into polarizabilities $\varepsilon = 15.4$, the volume $V \approx 549$ mm^3, $n = 2$ in equation (40)

In Fig. 10, one can notice that the solutions of the coupled dipole chain co-incide with the solutions for the chains of single dipoles at the Brillouin zone edge because the dipole sum $\widetilde{\Sigma_2}$, which is responsible for the interaction of magnetic and electric dipoles, turns zero. The solutions for the chains of single dipoles are the dashed lines in Fig. 10. The "ED mode" of the coupled dipole model tends to ω_{ED} curve [equation (55)], when "MD mode" to ω_{MD} one [equation (49)]. As we move away from the edge towards the centre of the Brillouin zone, the value of $\widetilde{\Sigma_2}$ increases, causing a repulsion between the dispersion branches. This results in an

increase in the group velocity of the first branch ("MD mode"), and the dispersion curve remains monotonic. However, unlike the first dispersion branch, the group velocity of the second branch ("ED mode") decreases and, as we will demonstrate, can even become negative, leading to a transition to a non-monotonic dispersion, even for the critical periods a_{crit} larger than $0.24\lambda_e$ for the single dipole chains.

From Fig. 10, it can be observed that both dispersion branches approach the resonant frequencies ω_m and ω_e of a single nanoresonator at the Brillouin zone edge. As a result, the intensity of the repulsion between these branches can be easily manipulated by controlling the relative positions of ω_m and ω_e. That is why it is interesting to analyze the behaviour of the dispersion branches for different ω_m and ω_e. For example, we can fix the frequency ω_e and vary the frequency ω_m. The results of the simulation with such parameters are presented in Fig. 11a). In this picture, we observe three pairs of branches corresponding to three values of ratios $r \equiv \omega_m/\omega_e = 0.62, 0.83, 0.95$. Other parameters of the simulation stay the same. Fig. 11 b) depicts the cross-section of the electric dipole using the model polarizability in equation (43) with the resonant frequency mentioned above and cross-sections of the magnetic dipole for 3 different ω_m calculated using an approximation in equation (40). One can notice that the bigger the ratio r, the closer the resonant frequencies to each other, and the bigger the overlap between magnetic and electric dipole cross-sections. Moreover, the maximum value of the magnetic cross-section is decreasing when frequencies become closer, indicating the energy transfer between magnetic and electric dipole modes. This means that the closer ω_m and ω_e to each other, the stronger will be the interaction between "ED modes" and "MD modes". Indeed, in Fig. 11 a) the pair of two branches corresponding to the frequency ratio 0.62, when the frequencies are quite far from each other, are monotonic and their behaviour is similar to the behaviour of two separated chains of magnetic and electric resonators (see Fig. 8 and Fig. 9). However, if we bring frequencies closer to one another, we notice that the branches change their behaviour. For $r = 0.83$, the dispersion curves come closer to each other at the edge of the Brillouin zone, which can be explained by the convergence of their frequencies. However, at the center of the Brillouin zone, the branches start to repulse, and the group velocity of the "ED mode" changes. In Fig. 11 c), a closer look at the upper branch for the ratio $r = 0.83$ is presented. One can notice that the dispersion became nonmonotonic. This result is particularly interesting since,
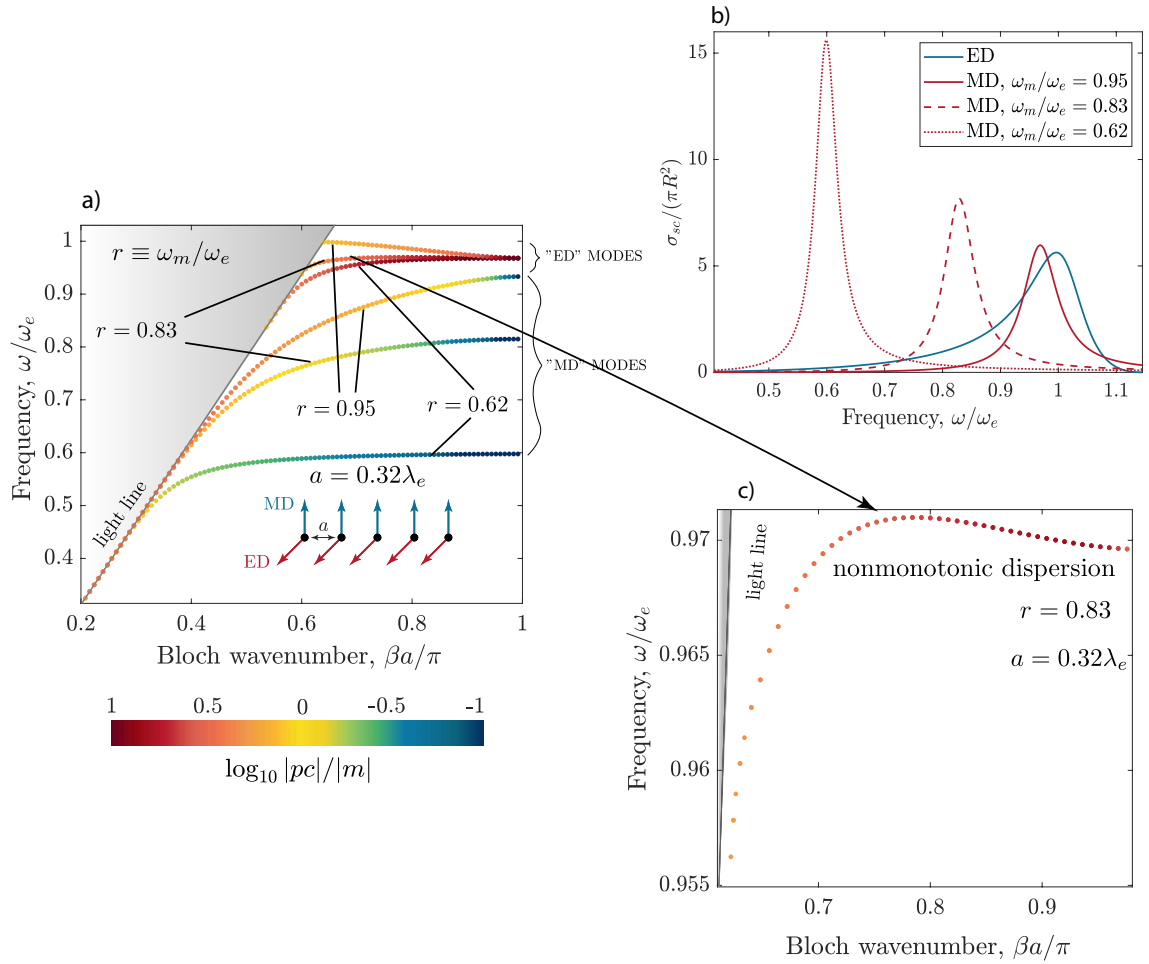
Figure 11 – a) Solution of the eigenproblem in equation (60) in the dipole model for the chain of coupled magnetic and electric dipoles. Parameters of the simulation are $\omega_e = 5.8 \cdot 10^{10}$ rad/s, $Q_m = 13$, $\omega_{e2} = 6.4 \cdot 10^{10}$ rad/s, $a = 10.3$ mm (the period of the chain), the relative permittivity of the resonator, which properties are incorporated into polarizabilities $\varepsilon = 15.4$, the volume $V \approx 549$ mm^3. The ratios between resonant magnetic and electric dipole frequencies, $\omega_m/\omega_e \equiv r$ equal to $0.62, 0.83, 0.95$. The horizontal axis corresponds to the Bloch wave number multiplied by the factor a/π, and the vertical axis corresponds to the frequency ω divided by the resonant frequency of the electric dipole of a single resonator ω_e. The gray area corresponds to the states above the light line. The colorbar represents the ratio $|pc/m|$ of the eigenvectors for three pairs of the dispersion branches. c) The nonmonotonic dispersion branch for the "ED mode" with $r = 0.83$. b) Cross-sections calculated using the approximations of α^H [equation (40)] and α^E [equation (43)]. The blue curve corresponds to the electric dipole, and the 3 red curves correspond to the magnetic dipole with 3 different ω_m listed in the legend of the plot. $n = 2$ in equation (40)

for the chains of single dipoles, we obtained that the maximal period for which the dispersion can be nonmonotonic is 0.24λ, however, here the period of the chain is equal to $0.32\lambda_e$. If we now make the frequencies almost equal to each other,

$\omega_m \approx \omega_e$ ($r = 0.95$), we observe further repulsion of two branches. Furthermore, one could notice that the bigger the ratio, the closer the values of $log_{10} \left| \dfrac{pc}{m} \right|$ to zero or $pc \approx m$ for both branches, which means that both magnetic and electric dipole moment contribute equally to the eigenstate vector when $\omega_m \approx \omega_e$. Hence, we can conclude that changing the ratio between resonant frequencies can greatly alter the behaviour of the dispersion curves.
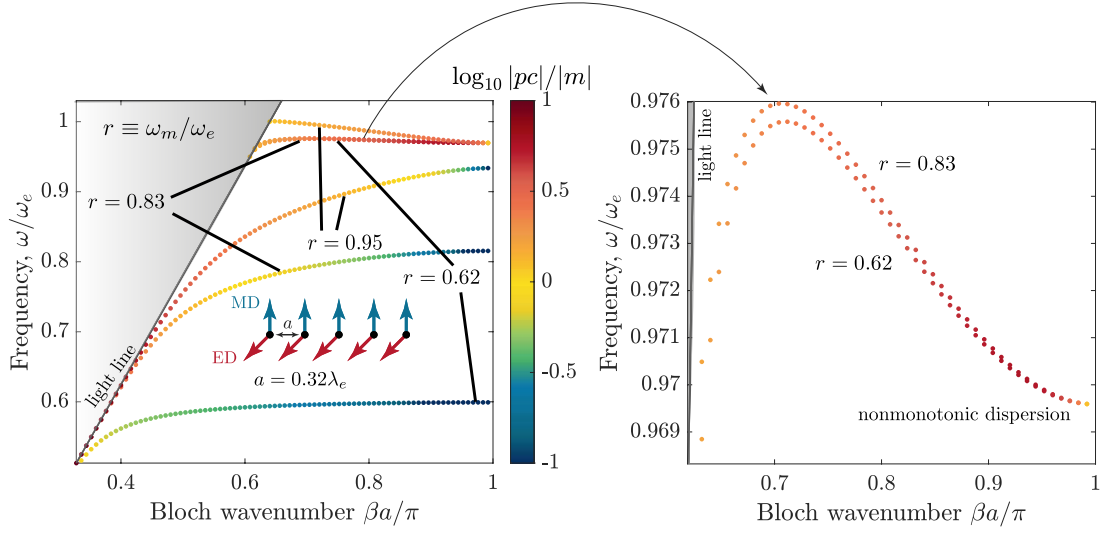

Figure 12 – Solution of the eigenproblem in equation (60) in the dipole model for the chain of coupled magnetic and electric dipoles. Parameters of the simulation are $\omega_e = 5.8 \cdot 10^{10}$ rad/s, $Q_m = 13$, $\omega_{e2} = 6.4 \cdot 10^{10}$ rad/s, $a = 10.3$ mm (the period of the chain), the relative permittivity of the resonator, which properties are incorporated into polarizabilities $\varepsilon = 15.4$, the volume $V \approx 549$ mm^3. The ratios between resonant magnetic and electric dipole frequencies, $\omega_m/\omega_e \equiv r$ equal to $0.62, 0.83, 0.95$. The horizontal axis corresponds to the Bloch wave number multiplied by the factor a/π, and the y-axis corresponds to the frequency ω divided by the resonant frequency of the electric dipole of a single resonator ω_e. The gray area corresponds to the states above the light line. The colorbar represents the ratio $|pc/m|$ of the eigenvectors for three pairs of dispersion branches. $n = 4$ in equation (40)

It is important to note that in all previous considerations in this section, $n = 2$ in the expression for the inversed magnetic dipole polarizability (40): $\frac{6\pi}{k_0^3 \alpha^H} = \frac{\omega_m - \omega}{\gamma_m} \left(\frac{\omega_m}{\omega} \right)^n - i$. Let us now analyze the behaviour of two dispersion branches for the same parameters but for $n = 4$. The simulation results are presented in Fig. 12. One can notice that the dispersion branches for $r = 0.62$ and $r = 0.83$ are now very close to each other, and almost indistinguishable. Moreover, in this case, the dispersion curve of the "ED mode" is already nonmonotonic for rather a small ratio of frequencies $r = 0.62$, whereas this dispersion branch was

monotonic for the case considered in Fig. 11. At the same time, the "MD dipole" branches did not change compared to the case in Fig. 11. This phenomenon could be explained with Fig. 13. In this picture, it is shown that, for $\omega_m \ll \omega_e$, the overlap between the cross-sections is getting bigger instead of getting smaller. This happens because the cross-section of the magnetic dipole starts to grow too fast at frequencies bigger than the resonant one due to the fourth power of the factor ω_m/ω in the reversed polarizability. Moreover, in reality, for such a small ratio as $\omega_m/\omega_e = 0.4$, higher-order dipole resonances as well as resonances of higher-order multipoles are definitely going to appear. This means that for the smaller ratios of frequencies, the first two dipole resonances would not interact with each other. This makes the model of magnetic dipole polarizability with $n = 4$ applicable in a small frequency range when magnetic and electric dipole resonances are relatively close to each other. Hence, despite the fact that the approximation with $n = 4$ works better than for $n = 2$ near the resonance (see section 1.3), overall, the $n = 2$ is better. In comparison with the model with $n = 2$, we saw that the smaller the ratio, the smaller the overlap.
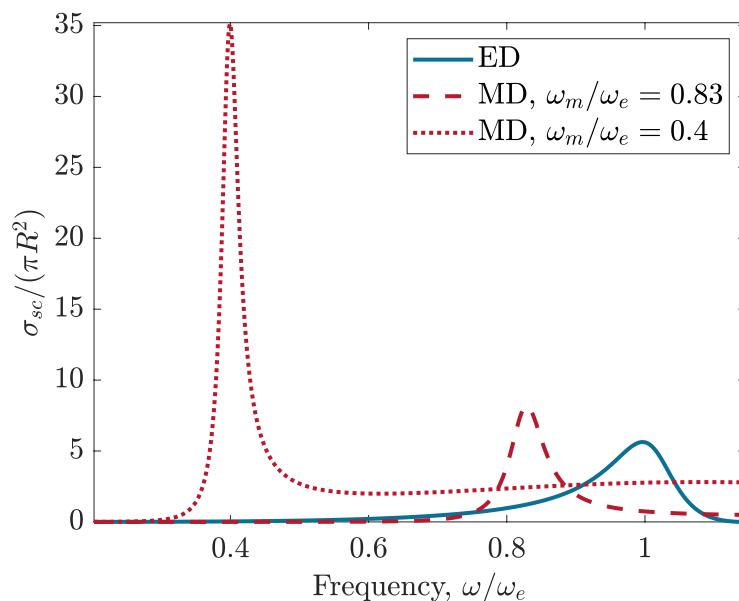

Figure 13 – Cross-sections for a single resonator calculated using the approximations of α^H [equation (40)] and α^E [equation (43)]. The blue curve corresponds to the electric dipole, and the two red curves correspond to the magnetic dipole with 2 different ω_m listed in the legend of the plot. $n = 4$ in equation (40)

We could also compare the dependence of maximal periods, when the dispersion is still nonmonotonic, $a_{\text{crit}}/\lambda_e$, for the cases of $n = 2$ and $n = 4$. In Fig.

14, one can see that, for $n = 2$, the critical period is increasing with the growth of the ratio between frequencies, while for $n = 4$ the dependence has a minimum. The results for $n = 2$ make more physical sense, since the smaller the ratios, the closer the values of the period to the case of only electric dipoles in the chain. This is logical since the further the frequencies, the less impact should their interaction have on the dispersion behaviour. In contrast, in the model of the magnetic polarizability with $n = 4$, the interaction is the strongest for the greatly detuned frequencies ($\omega_m/\omega_e = 0.4$). However, for the ratios between 0.75 and 0.9, the critical periods in the two cases are almost the same, which means that the model with $n = 4$ works well in that region. However, in our further considerations, we will rely on the model with $n = 2$.
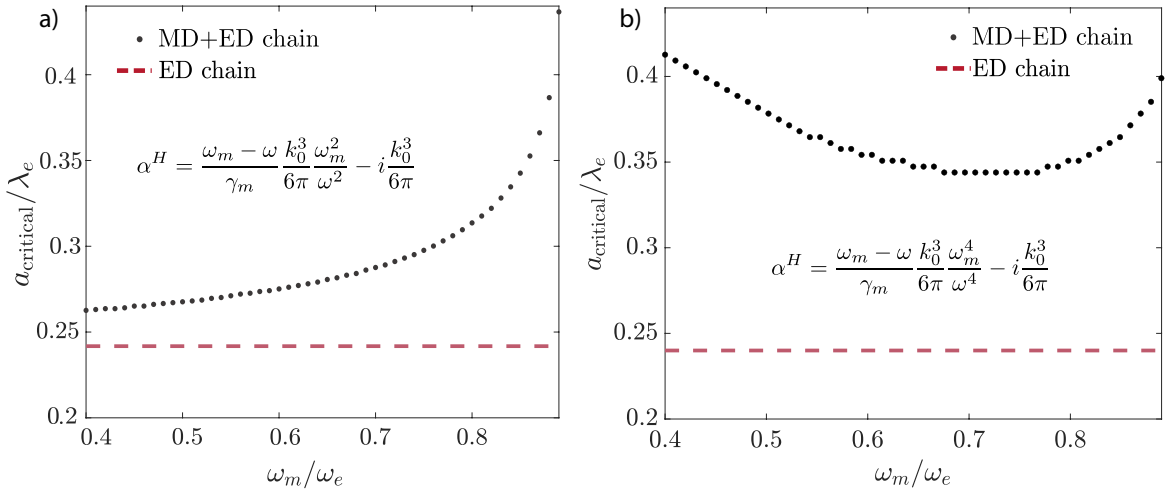

Figure 14 – The dependence of the maximal period (a_{crit}), for which the "ED mode" is still nonmonotonic on the ratio of the resonant magnetic and electric dipole frequencies ω_m/ω_e for n in equation (40) equal to a) 2, b) 4 compared to the critical period of the chain with only electric dipole response

Another important conclusion can be drawn from Fig. 14 a). As was discussed in previous sections for the chains with only one type of dipole, the critical period is around 0.24λ, which cannot be achieved for realistic nanoresonators. However, when considering the interactions of two dipoles, the critical period starts to grow and reaches $0.3\lambda_e$ around $\omega_m/\omega_e = 0.75$. This means that for the ratios higher than 0.75, the model can predict the properties of the chains of realistic nanoresonators. Although the ratio of frequencies of dipole resonances is fixed for spherical nanoresonators, we have more degrees of freedom with cylindrical, cubic and other shaped nanoresonators. For example, by changing the aspect ratio of the cylinder, we can achieve the desired shift of the resonant frequencies. That

is why it was very important to evaluate the applicability of the model for spherical particle polarizabilities in the case of a cylinder.

1.7 Comparison with COMSOL Multiphysics

In this section, we will compare the results of the dispersion calculation obtained using the dipole model and using full-wave simulation software COMSOL Multiphysics.

Let us first compare the results for the chain of spherical particles. In Fig. 15a), we can observe two dispersion branches, and both of them are monotonic. Note that for this case, the period of the chain is equal to 12 mm, which makes it around $0.5\lambda_e$. In Fig. 14, we saw that for the frequencies' ratio equal to 0.75 like for the sphere in our case, the maximal period, for which the dispersion of the upper branch in still nonmonotonic is around $0.3\lambda_e$ explaining the dispersion behaviour. Note that another disadvantage of using spherical particles instead of cylindrical ones is that for the chain of spherical particles, the periods will be always larger than the sphere diameter $2R$. At the same time, for the chain of cylinders with the configuration presented in the inset of Fig. 15, we have more degrees of freedom being able to adjust the aspect ratio of the cylinder while keeping the initial positions of the resonances. If we now compare the analytical results with the results obtained from full-wave simulation in Fig. 15b), we notice that the magnetic dispersion branch is in good agreement with analytical results in the range of normalized Bloch vectors from 1 to 0.75. Note that, in the type of structures that we are considering at low frequencies, the fundamental mode coincides with the plane wave, which means that the fundamental mode of the structure (or more specifically the "MD mode") should converge to the plane wave at low frequencies. For the smaller wavelength, the "MD mode" from dipole model faster converges to its asymptotics, namely the light line. This arguably happens because in the model of magnetic dipole polarizability in equation (40), we implemented a power factor, which made the magnetic dipole cross-section die down fast at low frequencies. Moreover, it is important to understand that we used a rough approximation of the polarizability because our goal is not to calculate the dispersion exactly but to predict the properties of the systems of nanoresonators easily varying their parameters, which would take a much longer time with the full-wave simulation. This means that such dissimilarities in the results do not interfere with our goal, and overall we admit the model describes the behaviour of the dispersion well.
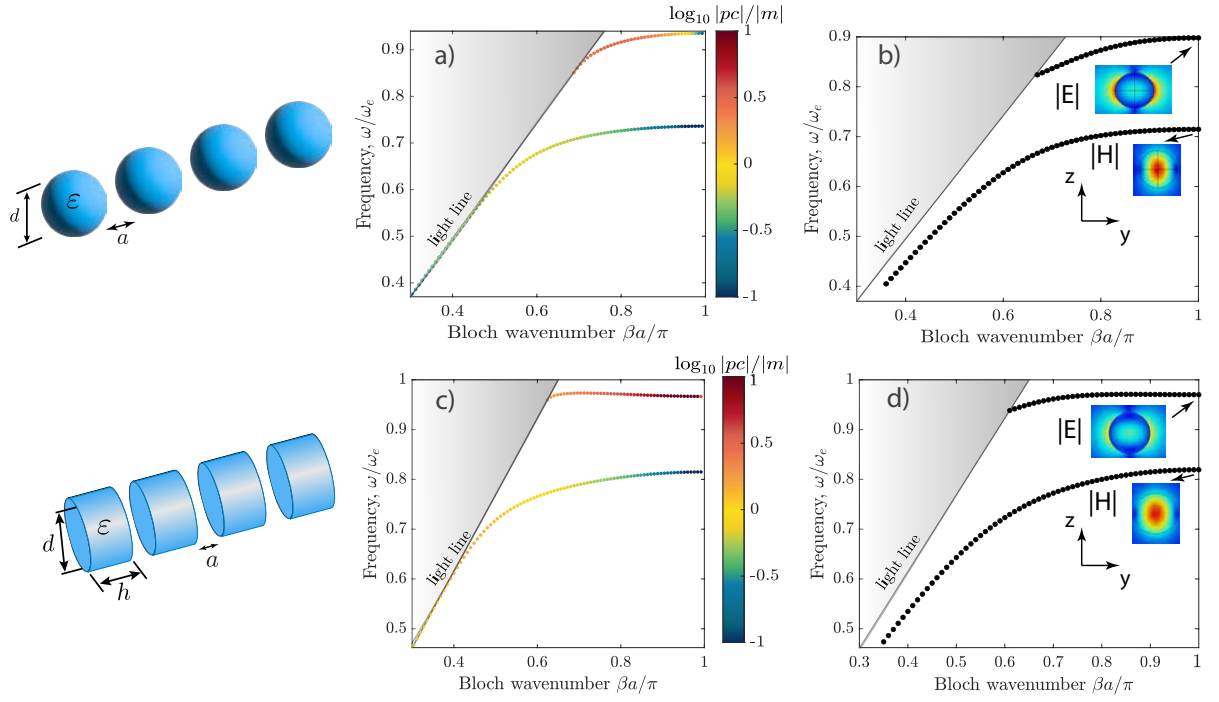
Figure 15 – a), c) Solution of the eigenproblem in equation (60) in the dipole model for the chain of coupled magnetic and electric dipoles. Parameters of the simulation are a) $\omega_e = 6.4 \cdot 10^{10}$ rad/s, $Q_m = 13$, $\omega_{e2} = 7.1 \cdot 10^{10}$ rad/s, $a = 12$ mm (the period of the chain), $\omega_m/\omega_e = 0.75$, b) $\omega_e = 5.8 \cdot 10^{10}$ rad/s, $Q_m = 13$, $\omega_{e2} = 6.4 \cdot 10^{10}$ rad/s, $a = 10.5$ mm (the period of the chain), $\omega_m/\omega_e = 0.83$. The relative permittivity of the resonators (spheres or cylinders), which properties are incorporated into polarizabilities, is $\varepsilon = 15.4$, the geometrical parameters are a) $d = 10$ mm, b) $d = 10$ mm, $h = 7$ mm. The colorbar represents the ratio $|pc/m|$ of the eigenvectors for the dispersion branches. $n = 2$ in equation (40) . b), d) The dispersion calculated in COMSOL Multiphysics with the same parameters as in the dipole model for the chain of spherical (b) and cylindrical nanoresonators (d). The insets show the distribution of the modulus of the electric field for the upper branch, and of the modulus of the magnetic field for the lower branch at the edge of the Brillouin zone. The horizontal axis corresponds to the Bloch wave number multiplied by the factor a/π, and the vertical axis corresponds to the frequency ω divided by the resonant frequency of the electric dipole of a single resonator ω_e. The gray area corresponds to the states above the light line

As for the upper branch, we see that the values of the frequencies are bigger in the dipole model for each value of the Bloch vector, but, in general, the behaviour is similar. This could potentially be explained by the presence of the strong quadrupole response near electric dipole resonance, which was shown in Fig. 4. The electric quadrupole contribution is not included in the model, however, it affects the "ED mode" dispersion.

41

If we now consider the chain of cylindrical particles with the period 10.5 mm, we observe that the "ED" branch is nonmonotonic for both COMSOL and dipole model calculations. For the "MD mode", the discussion is the same as for the case of spheres. However, here, for both branches, behaviour and frequencies' values in COMSOL and in the dipole model coincide, which makes us assume that the dipole model works better for the case of the cylinder due to the absence of the high-Q resonances of the magnetic quadrupole in the "dipole" frequency range.

One could also look at the insets in Fig. 15 with the field distributions simulated using COMSOL Multiphysics. The field distributions are calculated for the Bloch vector at the edge of the Brillouin zone. The distribution of the electric field magnitude for the upper branch shows that this mode corresponds to the electric dipole along y, while the magnetic field magnitude for the lower branch corresponds to the field distribution of the magnetic dipole along z. This is further proof of the applicability of our model to the considered systems. Indeed within our model, we can solve the dispersion equation constructed assuming that the magnetic dipole for each resonator is oriented along z and the electric dipole is oriented along y.

2 Theoretical description of the finite chain of nanoresonators with simultaneous magnetic and electric dipolar responses

2.1 System of equations describing the properties of the finite chain

In this section, we will analyze the behaviour of the finite chains of dielectric nanoresonators with magnetic and electric dipole responses. In particular, this analysis is important, since in practice, we can work only with finite-sized systems. The analysis of the electromagnetic properties of the infinite chain can only serve as a basis for the prediction of the properties of the finite chains.

As it was already mentioned above, we consider the chain of dielectric nanoresonators placed along the x-axis, with the magnetic dipole along the z-axis and the electric dipole along the y-axis. The interaction between dipoles can be expressed using Green's function [see section 1.1]. In contrast to the case of the infinite chain, the dipole sums for the finite chain in equation (28) and equation (31) are finite. Moreover, the Bloch theorem is not applicable to the electric and magnetic dipole moments of nanoresonators due to the lack of translational symmetry.

Using equation (28) and equation (31), let us construct the system of equations that will be solved below in order to find the eigenmodes and their energies for the finite chain:

$$
\begin{cases}
\dfrac{m^1}{\alpha^H} - k_0^2 \sum_{l=2}^{N} G_{zz}\left(0, |1-l|a\right) m^l + ik_0 c \sum_{l=2}^{N} G_{zy}^{HE}\left(0, (1-l)a\right) p^l = 0 \\[2mm]
\dfrac{(p^1 c)\varepsilon_0}{\alpha^E} - k_0^2 \sum_{l=2}^{N} G_{yy}\left(0, |1-l|a\right) (p^l c) - ik_0 \sum_{l=2}^{N} G_{yz}^{HE}\left(0, (1-l)a\right) m^l = 0 \\[2mm]
\vdots \\[2mm]
\dfrac{m^j}{\alpha^H} - k_0^2 \sum_{l=1,\neq j}^{N} G_{zz}\left(0, |j-l|a\right) m^l + ik_0 c \sum_{l=1,\neq j}^{N} G_{zy}^{HE}\left(0, (j-l)a\right) p^l = 0 \\[2mm]
\dfrac{(p^j c)\varepsilon_0}{\alpha^E} - k_0^2 \sum_{l=1,\neq j}^{N} G_{yy}\left(0, |j-l|a\right) (p^l c) - ik_0 \sum_{l=1,\neq j}^{N} G_{yz}^{HE}\left(0, (j-l)a\right) m^l = 0 \\[2mm]
\vdots
\end{cases}
,
$$

(63)

where a is the period of the chain, N is the number of nanoresonators in the chain, m^j, p^j are the values of magnetic and electric dipoles of the j-th nanoresonator,

respectively, c is the speed of light, k_0 is the wave number in free space. We also used that $\widehat{\mathbf{G}}(ja, la) = \widehat{\mathbf{G}}(0, |l-j|a)$. Let us now rewrite this equation in a matrix form:

$$\mathbf{M}\mathbf{d}_{em} = 0, \tag{64}$$

where $\mathbf{d}_{em} = (m^1, m^2, \dots, m^N, p^1 c, p^2 c, \dots, p^N c)^T$ is the vector of $2N$ dipole moments, , and $\mathbf{M}$ is $2N \times 2N$ interaction matrix. For convenience, we enumerate magnetic dipoles from 1 to N and electric dipoles from $N+1$ to $2N$. For better understanding, firstly, we draw a sketch of the matrix that we are considering, which is presented in Fig. 16. Now, we can define the components of the matrix

Figure 16 – The eigenvalue equation for the chain of N coupled magnetic and electric dipoles in matrix form

$\mathbf{M}$ starting from the diagonal components of the "MD-MD" domain of the matrix. Note that all the diagonal components of the matrix contain only the term with polarizability. For convenience, let us also multiply all the equations by $\dfrac{6\pi}{k_0^3}$, then:

$$M_{jj} = \frac{6\pi}{\alpha^H k_0^3} = \frac{\omega_m - \omega}{\gamma_m} \frac{\omega_m^n}{\omega^n} - i, \quad j \leqslant N. \tag{65}$$

Using the same considerations, we can also define the diagonal elements in the "ED-ED" block:

$$M_{jj} = \frac{6\pi\varepsilon_0}{\alpha^E k_0^3} = C_0 \frac{1 - \omega/\omega_e}{1 - \omega/\omega_{e2}} - i, \quad j \geqslant N+1. \tag{66}$$

The non-diagonal terms in the "MD-MD" block connect the magnetic dipole with the field of another magnetic dipole, hence:

$$
M_{jl} = -k_0^2 \frac{6\pi}{k_0^3} G_{zz}\left(0, |j-l|a\right) =
$$

$$
= -\frac{3}{2} e^{ik_{jn}} \left(\frac{1}{k_{jn}} + \frac{i}{k_{jl}^2} - \frac{1}{k_{jl}^3} \right) \equiv C_{jl}, \quad j \leqslant N, l \leqslant N,
$$

(67)

where $k_{jn} = k_0 d |j-n|$. The non-diagonal components of the "ED-ED" block of **M**, which connect the electric dipole with the field of another electric dipole are:

$$
M_{jl} = -k_0^2 \frac{6\pi}{k_0^3} G_{yy}\left(0, |j-l|a\right) =
$$

$$
= -\frac{3}{2} e^{ik_{jn}} \left(\frac{1}{k_{jn}} + \frac{i}{k_{jl}^2} - \frac{1}{k_{jl}^3} \right) = C_{jl}, \quad N+1 \leqslant j \leqslant 2N, N+1 \leqslant l \leqslant 2N.
$$

(68)

The components of the "MD-ED" block of **M**, which connect the magnetic dipole with the field of an electric dipole are:

$$
M_{jl} \stackrel{r=l-N}{=} ik_0 G_{zy}^{HE}\left(0, (j-r)a\right) = -\frac{3}{2} e^{ik_{rj}} \left(\frac{1}{k_{rj}} + \frac{i}{k_{rj}^2} \right) sgn(j-r)
$$

$$
\equiv D_{jr} \frac{r-j}{|r-j|}, j \leqslant N, N+1 \leqslant l \leqslant 2N,
$$

(69)

where $D_{jr} \equiv \frac{3}{2} e^{ik_{rj}} \left(\frac{1}{k_{rj}} + \frac{i}{k_{rj}^2} \right)$. We define the components of the "ED-MD" block of the matrix **M** in the same manner:

$$
M_{jl} \stackrel{r=j-N}{=} -ik_0 G_{yz}^{HE}\left(0, (r-l)a\right) = -\frac{3}{2} e^{ik_{rl}} \left(\frac{1}{k_{rl}} + \frac{i}{k_{rl}^2} \right) sgn(r-l)
$$

$$
= D_{rl} \frac{l-r}{|l-r|}, l \leqslant N, N+1 \leqslant j \leqslant 2N.
$$

(70)

In the end, we obtain the following matrix:

$$
M_{jl} = \begin{cases}
\dfrac{\omega_m - \omega}{\gamma_m} \dfrac{\omega_m^n}{\omega^n} - i, & \text{if } l = j \leqslant N \\[2ex]
C_0 \dfrac{1 - \omega/\omega_e}{1 - \omega/\omega_{e2}} - i, & \text{if } l = j > N \\[2ex]
C_{jl}, & \text{if } l \neq j,\ j,l \leqslant N \text{ or } j,l > N \\[2ex]
D_{rl} \dfrac{l - r}{|l - r|}, & \text{if } l \neq r,\ r,l \leqslant N,\ r = j - N \\[2ex]
D_{jr} \dfrac{r - j}{|r - j|}, & \text{if } r \neq j,\ r,j \leqslant N,\ r = l - N
\end{cases}
\tag{71}
$$

We now need to rewrite the equation (64) to obtain the eigenvalue problem of the following form:

$$
\mathbf{X} \mathbf{d}_{em} = \omega \mathbf{Y} \mathbf{d}_{em},
\tag{72}
$$

where $\mathbf{X}, \mathbf{Y}$ are $2N \times 2N$ matrices. Note that for the case of the finite chain, the eigenfrequencies ω are complex-valued.

We will solve our problem in quasi-resonant approximation around the resonant frequency of either magnetic or electric dipole. In this way, only the polarizabilities α^H and α^E depend on frequency. In the previous chapter, we discovered that the electric dipole dispersion branch has an inflection point for a certain parameter set, therefore, we will take ω_e for the resonant frequency and evaluate the elements of matrices $\mathbf{X}, \mathbf{Y}$ at this frequency.

To obtain the eigenproblem in a form in equation (72), we multiply the lower half of the matrix $\mathbf{M}$ by the factor $1 - \omega/\omega_{e2}$, and obtain the following equation:

$$
\hat{\mathbf{I}} \otimes \begin{pmatrix} \dfrac{\omega_m}{\gamma_m} \dfrac{\omega_m^n}{\omega_e^n} - i & 0 \\[2ex] 0 & C_0 - i \end{pmatrix} + \hat{\mathbf{A}} = \dfrac{\omega}{\gamma_m} \left(\hat{\mathbf{I}} \otimes \begin{pmatrix} \dfrac{\omega_m^n}{\omega_e^n} & 0 \\[2ex] 0 & \dfrac{C_0 \gamma_m}{\omega_e} - \dfrac{i \gamma_m}{\omega_{e2}} \end{pmatrix} + \hat{\mathbf{B}} \right),
\tag{73}
$$

where $\hat{\mathbf{I}}$ is the $N \times N$ identity matrix, and

$$
A_{jl} = \begin{cases}
C_{jl}, & \text{if } l \neq j,\ j,l \leqslant N \\[6pt]
C_{jl}, & \text{if } l \neq j,\ j,l > N \\[6pt]
D_{rl}\dfrac{l-r}{|l-r|}, & \text{if } l \neq r,\ r,l \leqslant N,\ r = j - N \\[6pt]
D_{jr}\dfrac{r-j}{|r-j|}, & \text{if } r \neq j,\ r,j \leqslant N,\ r = l - N, \\[6pt]
0,\ \text{otherwise}
\end{cases}
\tag{74}
$$

$$
B_{jl} = \begin{cases}
\dfrac{\gamma_m}{\omega_{e2}}C_{jl}, & \text{if } l \neq j,\ j,l > N \\[8pt]
\dfrac{\gamma_m}{\omega_{e2}}D_{rl}\dfrac{l-r}{|l-r|}, & \text{if } l \neq r,\ r,l \leqslant N,\ r = j - N \\[8pt]
0,\ \text{otherwise.}
\end{cases}
\tag{75}
$$

One can see that all the matrix equation components are dimensionless, which is necessary for numerical simulations. Moreover, note that we will search for the normalized eigenvalues ω/γ_m, hence, we will need to multiply the result by γ_m to find the actual frequency. All the following considerations are made assuming the power $n = 2$ in the magnetic dipole polarizability model in equation (40).

2.2 Numerical simulations

In this section, we will solve equation (73) for different N and different frequencies' ratios. We are going to analyze the Q-factors of the modes for each N. As was already discussed in the introduction, the Q-factors of the finite chains with the parameters, for which in the infinite chain the dispersion is nonmonotonic, is scaling as $N^\alpha, \alpha \approx 7$. Thus, in our case, at frequencies around ω_e, we expect high values of the quality factor. The Q-factor can be obtained using the following formula:

$$
Q = -\frac{\mathrm{Re}(f_0)}{2\mathrm{Im}(f_0)},
\tag{76}
$$

where f_0 is the eigenmode frequency related to the angular eigenfrequency ω as $f_0 = \omega/2\pi$. For each N, there are $2 \times N$ modes where half of them has frequencies around ω_e and another half has around ω_m. Thus, in the finite chain, we also have the splitting of all modes into "MD modes" and "ED modes".
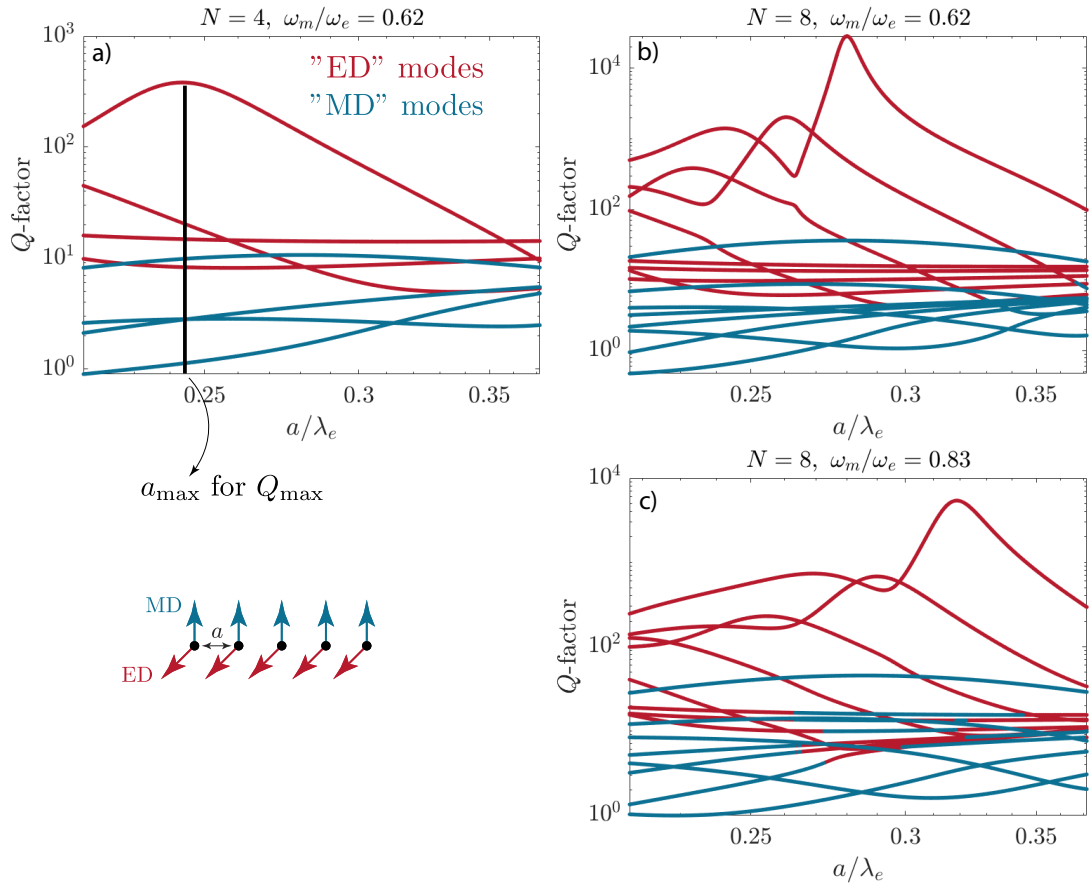
Figure 17 – Dependence of the Q-factor on the chain period a normalized by the resonant wavelength λ_e of the electric dipole. The "ED modes" and "MD modes" are divided by colour. Parameters of the simulation are $\omega_e = 5.8 \cdot 10^{10}$ rad/s, $Q_m = 13$, $\omega_{e2} = 6.4 \cdot 10^{10}$ rad/s, the relative permittivity of the resonator, which properties are incorporated into polarizabilities $\varepsilon = 15.4$, the volume $V \approx 549$ mm^3. The ratio between magnetic and electric frequencies and the number of the nanoresonators N are as follows a) $\omega_m/\omega_e = 0.62$, $N = 4$, b) $\omega_m/\omega_e = 0.62$, $N = 8$, c) $\omega_m/\omega_e = 0.62$, $N = 8$

The results of the simulations for the ratios $\omega_m/\omega_e = 0.62, 0.83$ are presented in Fig. 17. Other parameters of the simulation are listed in the caption. In this figure, we observe the dependence of Q-factors for all modes on the chain period a. For the ratio $\omega_m/\omega_e = 0.62$, the separation into "MD modes" and "ED modes" can be conducted easily since ω_e and ω_m have large detuning. However, in Fig. 17c), for the ratio $\omega_m/\omega_e = 0.83$, the modes with the low Q-factors are mixed up since ω_e is relatively close to ω_m. Nevertheless, we observe that, for all three cases, the modes with the highest Q-factors are "ED modes". This happens due to two factors: 1) the ED dispersion branch is nonmonotonic in the infinite chain with the same parameters; 2) we are solving the dispersion equation in quasi-resonant approximation around the electric dipole frequency.

Now, if we compare the results in Fig. 17a) and in Fig. 17b) for the same ratio ω_m/ω_e, but different N, we notice that the maximal Q-factor and the period $a_{\max}$, for which it occurs, is larger for the larger N. This is a good sign since we want to receive the scaling of the Q-factor as $N^\alpha, \alpha \approx 7$. To analyze the dependence of the Q-factors on the number of resonators, for each N, we will find the maximal Q-factor and the corresponding period $a_{\max}$, as it is demonstrated in Fig. 17. If one compares the results in Fig. 17b) and in Fig. 17c), one can notice that the period $a_{\max}$ is bigger in the case when the frequencies are closer to each other, however, the maximal Q-factor is smaller for the ratio 0.83 than for 0.62.

The dependence of the maximal Q-factor and $a_{\max}$ for different ω_m/ω_e on the number of particles N is presented in Fig. 18. One can notice that the power of N, which the Q-factor is scaling as is around $\alpha \approx 6.8$ for the cases in Fig. 18a), b), c) as it was predicted in Ref. [36] in the dipole model with only electric dipoles. Moreover, we see that the values of the periods $a_{\max}$ tend to be a certain asymptotic for all three cases. Since the bigger the number of particles, the closer the finite chain properties are to the properties of the infinite chain, one could compare this asymptotics with the critical periods received for every frequencies' ratios for the infinite chain in Fig. 14a). We see that, for instance, for $\omega_m/\omega_e = 0.62$, the critical period is around $0.27\lambda_e$, when in the finite chain we see that the periods with maximal Q-factor tend to $0.3\lambda_e$. Recall that the bent dispersion in the infinite chain serves as the basis for the formations of "high-Q" modes in the finite chains due to the destructive interference of two collective modes. This difference could be explained by the following fact. In order to solve the dispersion equation for the finite chain, we used quasi-resonant approximation in addition to the approximation of the polarizabilities used also for the infinite chain. One could notice that, as shown for the infinite chain, the periods are larger for the bigger ratios between the resonant frequencies. Moreover, for $\omega_m/\omega_e = 0.62$, it is shown that the dispersion is monotonic for the periods equal to $0.32\lambda_e$ (see Fig. 11). This means that for this value of the periods, there will not be any destructive interference of the collective modes and, hence, the Q scaling as N^7 is not attainable. And for the case of the finite chain, the asymptotic value for the periods for $\omega_m/\omega_e = 0.62$ is equal to $0.3\lambda_e$. The same considerations could be done for other ratios of frequencies presented in Figs. 18a), 18b), and 18c).
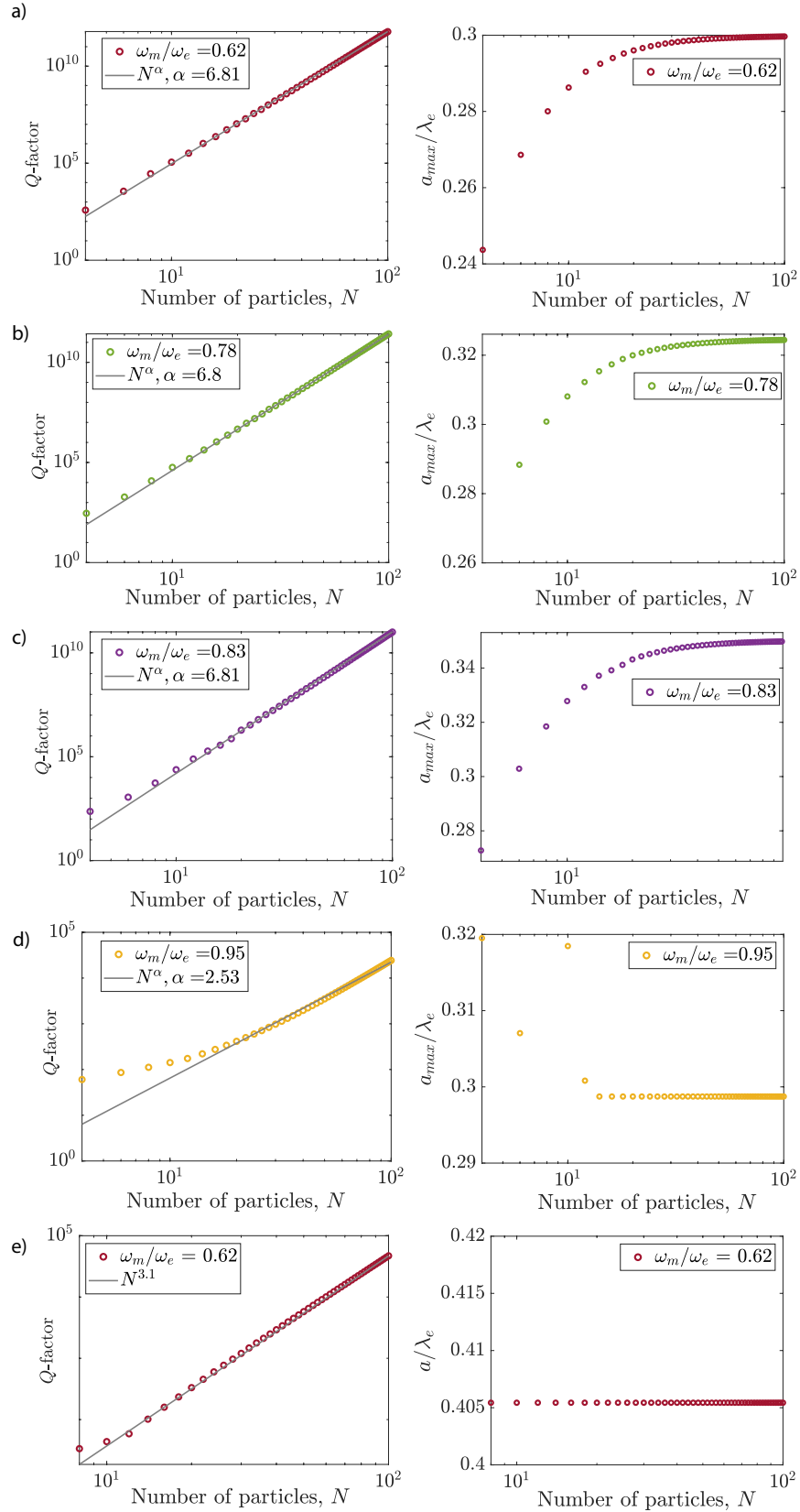
Figure 18 – Left panel: the dependence of the maximal Q-factor on the number of particles in the chain N for different frequencies ratios a), $\omega_m/\omega_e = 0.4$, b), e) $\omega_m/\omega_e = 0.62$, c) $\omega_m/\omega_e = 0.83$, d) $\omega_m/\omega_e = 0.95$; and the asymptotic N^α for each case. Right panel: the dependence of the period, for which the Q-factor is maximal, on the number of particles in the chain N

50

In Fig. 18d) for $\omega_m/\omega_e = 0.95$, we observe the drop of the power of N to $\alpha \approx 2.5$, and the periods a_{max} are smaller than for the smaller ratios. This could be explained by the fact that the quasi-resonant approximation may not work that well when the resonant frequencies are almost equal to each other. Moreover, in Fig. 11, we saw that the upper dispersion branch for $r = 0.95$ goes up and does not have an inflection point close to the Brillouin zone edge, which is the reason for the huge increase of the Q-factors.

If we now consider again the ratio of ω_m and ω_e equal to 0.62 but increase the periods to the values larger than $0.3\lambda_e$, we will see that the Q-factors are scaling as N^3, and the periods are staying at values around $0.4\lambda_e$ [see Fig. 18e)]. This is because, for such values of the periods, the dispersion branch for $\omega_m/\omega_e = 0.62$ in the infinite chain would be monotonic, which corresponds to the regular band-edge modes.

2.3 Comparison with COMSOL Multiphysics

In this section, we will compare the results of the finite chain analysis performed in the dipole model with the results obtained in COMSOL Multiphysics. To obtain the maximal value of the Q-factor for each value of N, one should calculate the Q-factors of all the modes of interest in a certain range of periods, which can be chosen using the dipole model. The results of the calculation of the Q-factor dependence on the chain period a for $N = 8$ and $\omega_m/\omega_e = 0.83$ are presented in Fig. 19. This figure presents the dependence of the Q-factors for three eigenmodes with the largest Q around frequency $\omega_e = 5.6$ rad/s. One can notice that the maximal value of the Q-factor is around 10^4, which is a lot for such a small number of particles. The period, at which such Q is obtained is $0.33\lambda_e$, which means, as already discussed, that $a \approx 0.24\lambda_e$ is not enough to describe the properties of the realistic resonators. If we compare the results for the same parameters in the dipole model in Fig. 17c), we see that the behaviour of the Q-factor curves as well as the values are similar to the dependence in Fig. 19.

In the inset of Fig. 19, one can see the distribution of the electric field modulus for the mode with the highest Q-factor. We note that the field is concentrated in the middle of the structure whereas it is almost zero at the edges. This behaviour is explained by the fact that this mode frequency is the closest one to the frequency at the band edge in the infinite structure, where the group velocity turns zero. Then, in the finite structure, the field is distributed like in a standing wave.
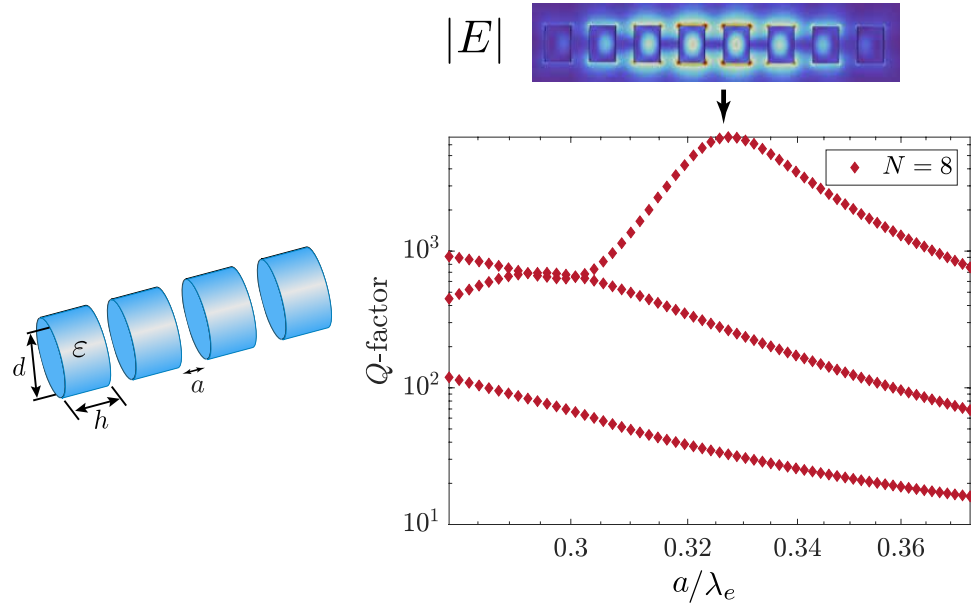
Figure 19 – The Q-factor dependence on the period of the dielectric cylinders chain a normalized by the resonant wavelength λ_e of the electric dipole. The axis of the chain coincides with the rotational axis of the cylinder. Parameters of the simulation are $R = 5$ mm, $h = 7$ mm, the relative permittivity $\varepsilon = 15.4$, $N = 8$ (number of the cylinders), $\omega_m/\omega_e = 0.83$. The inset shows the distribution of the electric field norm for the mode with the highest quality factor
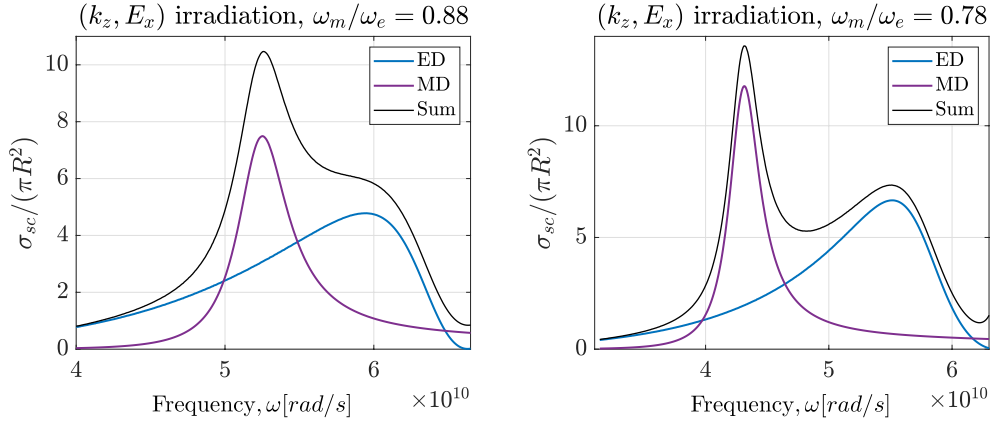

Figure 20 – Normalized scattering cross-section $\sigma_{sc}/(\pi R^2)$ and its multipole decomposition into electric dipole (ED), magnetic dipole (MD) terms normalized on the surface of the base of the cylinder-shaped nanoparticle. The incident plane wave is x-polarized and propagates along the z-axis. The parameters of the cylinder: a) diameter of the cylinder base $d = 10$ mm, the cylinder height $h = 6$ mm, b) $d = 10$ mm, the cylinder height $h = 9$ mm. The relative permittivity of the material is $\varepsilon = 15.4$

If we now want to compare the Q-factor dependence on the number of particles N for different ratios of frequencies, we should find the parameters of the

appropriate particles. Fig. 20 presents the multipole decomposition of scattering cross section for two cylinders with different heights. One can see that by changing the cylinder height, we can change the positions of the resonances, and, hence, the ratio ω_m/ω_e. Including the cylinder that we were considering previously, we now know the parameters of the cylinders with the following ratios: $\omega_m/\omega_e = 0.78, 0.83, 0.88$. For convenience, we create a table with all the parameters necessary for the dipole model calculations in table 1 for three different cylinders with different ratios of frequencies. The Q-factors of the single resonators were obtained using eigenmode calculation in COMSOL Multiphysics, and frequencies were obtained from cross-sections. We can now calculate the Q-factor dependence for all three cases in both the dipole model and COMSOL. The results of the simulations are presented in Fig. 21. In Fig. 21b) and Fig. 21c), one can see that for both COMSOL and the dipole model, the values of the Q-factors as well as the power of N are bigger for the smaller ratios. However, as we saw before in the dipole model, the Q-factors are scaling as $N^{6.8}$ for the same ω_m/ω_e. Here, the number of considered resonators is not enough to see the asymptotic behaviour. However, the calculations for the chains of more than 20 resonators in COMSOL are very time-consuming. We can assume that, in COMSOL, the power of N of the asymptotic will also grow to become N^α with $\alpha \approx 7$ similar to the dipole model. If we compare the periods, at which the maximal Q-factor is obtained, we observe that the periods in COMSOL are larger. Moreover, $a_{\max}$ are bigger for the ratio 0.78 than for the ratio 0.83, whereas, in the dipole model, the bigger the ratio, the larger the periods. However, in contrast to the dipole model, in COMSOL we calculate the dispersion of the realistic chain of nanoresonators, and their geometrical sizes matter. One can assume that because the height of the cylinder is larger for the ratio 0.78 than for 0.83, the periods of the structure for which we obtain modes with high Q are bigger. Moreover, for the calculations in the dipole model, we used the quasi-resonant approximation, which can also affect the results. In summary, we can conclude that the dipole model works well for predicting the formation of "high-Q" states in the chains of realistic resonators.

Table 1 – Table with the parameters of cylindrical nanoresonators with different frequency ratios ω_m/ω_e. R is the radius of the cylinder base, h is the cylinder height, ω_e is the frequency of the electric dipole resonance, ω_{e2} is the frequency of zero of electric dipole scattering

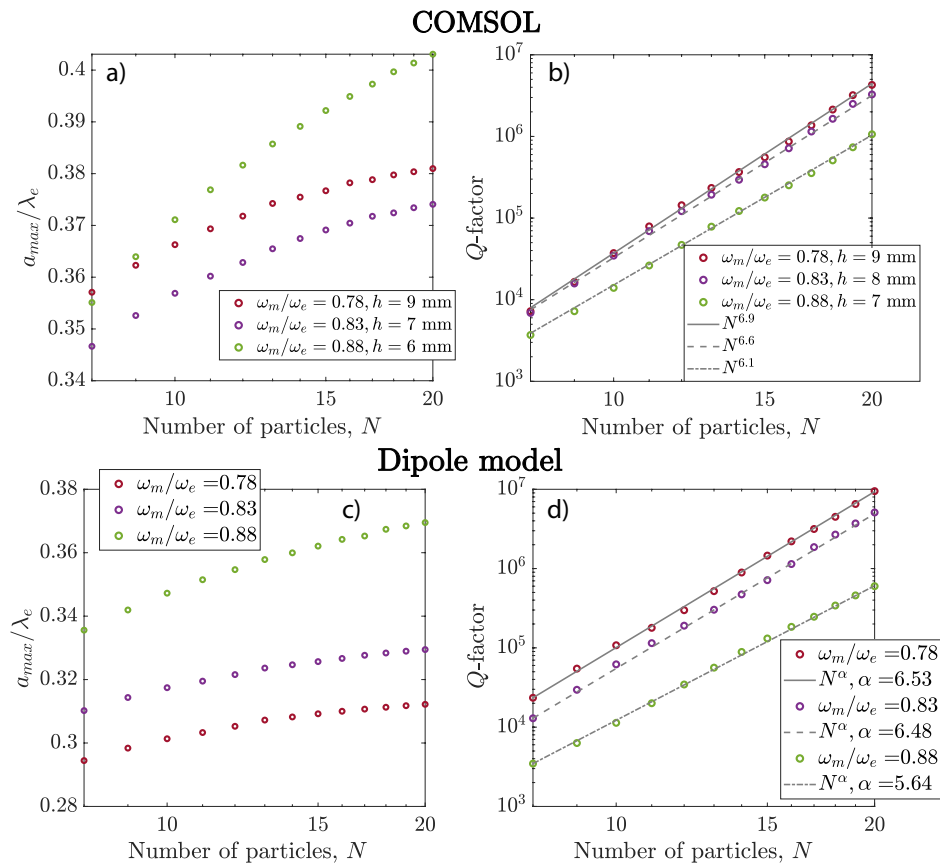|	$\dfrac{\omega_m}{\omega_e} = 0.78$	$\dfrac{\omega_m}{\omega_e} = 0.83$	$\dfrac{\omega_m}{\omega_e} = 0.88$
h [mm]	9	7	6
R [mm]	5	5	5
ω_e [rad/s]·10^{10}	5.52	5.79	5.95
ω_{e2} [rad/s]·10^{10}	6.48	6.34	6.63
Q_m	12.8	13.6	14.3

Figure 21 – The dependence of the maximal Q-factor on the number of cylinders in the chain N for different frequency ratios and the sizes of a nanoresonator: $\omega_m/\omega_e = 0.78$, $h = 9$ mm, $R = 5$ mm; $\omega_m/\omega_e = 0.63$, $h = 7$ mm, $R = 5$ mm; $\omega_m/\omega_e = 0.88$, $h = 6$ mm, $R = 5$ mm; and the asymptotic N^α for each case. Right panel: the dependence of the chain period, for which the Q-factor is maximal, on the number of particles in the chain N for different frequency ratios. The relative permittivity of the cylinder is 15.4. Results are obtained a), b) from COMSOL multiphysics and c), d) using the dipole model

CONCLUSION

In this work, we investigated theoretically and numerically the formation of "high-Q" band-edge modes in the chains of dielectric resonators with simultaneous magnetic and electric dipole responses. The mechanism of appearance of such modes lies in destructive interference of two collective modes in the finite chains of particles which becomes possible due to the bending of the dispersion in the infinite chains with the same parameters.

We formulated the system of equations for the chain of coupled electric and magnetic dipoles. To solve this equation, we first approximated magnetic and electric polarizabilities with simple analytical functions, which do not depend on the shape of the nanoresonator. Then, we solved the dispersion equation, and showed that the coupling between the electric and magnetic dipole modes in the infinite chains of particles leads to the repulsion of the dispersion branches. Moreover, by changing the ratio between resonant electric and magnetic frequencies of the single resonator of the structure, we can achieve the negative group velocity of the "ED mode", the frequency of which at the band edge is close to the one resonant of the electric dipole of the single resonator. Furthermore, the periods, for which such an effect occurs, are larger than 0.3λ for ratios between the magnetic and electric frequencies $\omega_m/\omega_e \geqslant 0.75$. The appearance of the nonmonotonic dispersion branch in the infinite systems leads to the dramatic increase of the Q-factors in the finite system, which, as we showed, scaling as N^7.

The dipole model with two types of dipole responses can easily predict the behaviour of the realistic systems, which was shown by a comparison of the results with the full-wave simulation software. We believe that our research findings have the potential to significantly enhance the existing approaches for designing high-Q compact resonators, which have already proven to have numerous applications such as lasing, sensing, and more.

REFERENCES

1 All-dielectric nanophotonics: the quest for better materials and fabrication techniques / D. G. Baranov [et al.] // Optica. — 2017. — Vol. 4, no. 7. — P. 814–825.

2 Pelton M., Aizpurua J., Bryant G. Metal-nanoparticle plasmonics // Laser Photonics Rev. — 2008. — Vol. 2, no. 3. — P. 136–159.

3 Plasmonic Nanoantennas: Fundamentals and Their Use in Controlling the Radiative Properties of Nanoemitters / V. Giannini [et al.] // Chem. Rev. — 2011. — Vol. 111, no. 6. — P. 3888–3912.

4 Optically resonant dielectric nanostructures / A. I. Kuznetsov [et al.] // Science. — 2016. — Vol. 354, no. 6314. — aag2472.

5 Towards all-dielectric metamaterials and nanophotonics / A. Krasnok [et al.] // Proceedings Volume 9502, Metamaterials X. Vol. 9502. — SPIE, 2015. — P. 950203.

6 Kivshar Y. All-dielectric meta-optics and non-linear nanophotonics // Natl. Sci. Rev. — 2018. — Vol. 5, no. 2. — P. 144–158.

7 Mie G. Beitrge zur Optik trber Medien, speziell kolloidaler Metallsungen // Ann. Phys. — 1908. — Vol. 330, no. 3. — P. 377–445.

8 Bohren C. F., Huffman D. R. Absorption and scattering of light by small particles. — John Wiley & Sons, 2008.

9 Demonstration of Magnetic Dipole Resonances of Dielectric Nanospheres in the Visible Region / A. B. Evlyukhin [et al.] // Nano Lett. — 2012. — Vol. 12, no. 7. — P. 3749–3755.

10 Optical response features of Si-nanoparticle arrays / A. B. Evlyukhin [et al.] // Phys. Rev. B. — 2010. — Vol. 82, no. 4. — P. 045404.

11 Alaee R., Rockstuhl C., Fernandez-Corbaton I. An electromagnetic multipole expansion beyond the long-wavelength approximation // Opt. Commun. — 2018. — Vol. 407. — P. 17–21.

12 Evlyukhin A. B., Reinhardt C., Chichkov B. N. Multipole light scattering by nonspherical nanoparticles in the discrete dipole approximation // Phys. Rev. B. — 2011. — Vol. 84, no. 23. — P. 235429.

13 High-Efficiency Dielectric Huygens' Surfaces / M. Decker [et al.] // Adv. Opt. Mater. — 2015. — Vol. 3, no. 6. — P. 813–820.

14 Transverse Scattering and Generalized Kerker Effects in All-Dielectric Mie-Resonant Metaoptics / H. K. Shamkhi [et al.] // Phys. Rev. Lett. — 2019. — Vol. 122, no. 19. — P. 193905.

15 Magnetic and electric coherence in forward- and back-scattered electromagnetic waves by a single dielectric subwavelength sphere / J. M. Geffrin [et al.] // Nat. Commun. — 2012. — Vol. 3, no. 1171. — P. 1–8.

16 All-Dielectric Huygens' Meta-Waveguides for Resonant Integrated Photonics / Y. D. Srmac [et al.] // Laser Photonics Rev. — 2023. — P. 2200860.

17 Chemically etched ultrahigh-Q wedge-resonator on a silicon chip / H. Lee [et al.] // Nat. Photonics. — 2012. — Vol. 6, no. 6. — P. 369–373.

18 Foreman M. R., Swaim J. D., Vollmer F. Whispering gallery mode sensors // Adv. Opt. Photonics. — 2015. — Vol. 7, no. 2. — P. 168–240.

19 High-Q Supercavity Modes in Subwavelength Dielectric Resonators / M. V. Rybin [et al.] // Phys. Rev. Lett. — 2017. — Vol. 119, no. 24. — P. 243901.

20 Gather M. C., Yun S. H. Single-cell biological lasers // Nat. Photonics. — 2011. — Vol. 5, no. 7. — P. 406–410.

21 Single nanoparticle detection using split-mode microcavity Raman lasers / B.-B. Li [et al.] // Proc. Natl. Acad. Sci. U.S.A. — 2014. — Vol. 111, no. 41. — P. 14657–14662.

22 Lasing action from photonic bound states in continuum / A. Kodigala [et al.] // Nature. — 2017. — Vol. 541, no. 7636. — P. 196–199.

23 Bulgakov E. N., Maksimov D. N. Topological Bound States in the Continuum in Arrays of Dielectric Spheres // Phys. Rev. Lett. — 2017. — Vol. 118, no. 26. — P. 267401.

24 Asymmetric Metasurfaces with High-Q Resonances Governed by Bound States in the Continuum / K. Koshelev [et al.] // Phys. Rev. Lett. — 2018. — Vol. 121, no. 19. — P. 193903.

25 Bound states in the continuum / C. W. Hsu [et al.] // Nat. Rev. Mater. — 2016. — Vol. 1, no. 16048. — P. 1–13.

26 Polarization Switching Between Electric and Magnetic Quasi-Trapped Modes in Bianisotropic All-Dielectric Metasurfaces / A. B. Evlyukhin [et al.] // Laser Photonics Rev. — 2021. — Vol. 15, no. 12. — P. 2100206.

27 Metasurface Engineering through Bound States in the Continuum / A. S. Kupriianov [et al.] // Phys. Rev. Appl. — 2019. — Vol. 12, no. 1. — P. 014024.

28 Bianisotropy for light trapping in all-dielectric metasurfaces / A. B. Evlyukhin [et al.] // Phys. Rev. B. — 2020. — Vol. 101, no. 20. — P. 205415.

29 Symmetric metasurface with dual band polarization-independent high-Q resonances governed by symmetry-protected BIC / Y. Cai [et al.] // Opt. Lett. — 2021. — Vol. 46, no. 16. — P. 4049–4052.

30 Collective Mie Resonances for Directional On-Chip Nanolasers / T. X. Hoang [et al.] // Nano Lett. — 2020. — Vol. 20, no. 8. — P. 5655–5661.

31 Figotin A., Vitebskiy I. Gigantic transmission band-edge resonance in periodic stacks of anisotropic layers // Phys. Rev. E. — 2005. — Vol. 72, no. 3. — P. 036619.

32 Coupling of Germanium Quantum Dots with Collective Sub-radiant Modes of Silicon Nanopillar Arrays / V. Rutckaia [et al.] // ACS Photonics. — 2021. — Vol. 8, no. 1. — P. 209–217.

33 Demonstration of the enhanced Purcell factor in all-dielectric structures / A. Krasnok [et al.] // Appl. Phys. Lett. — 2016. — Vol. 108, no. 21.

34 Degenerate band edge laser / M. Veysi [et al.] // Phys. Rev. B. — 2018. — Vol. 97, no. 19. — P. 195107.

35 Extremely subradiant states in a periodic one-dimensional atomic array / D. F. Kornovan [et al.] // Phys. Rev. A. — 2019. — Vol. 100, no. 6. — P. 063832.

36 High-Q Localized States in Finite Arrays of Subwavelength Resonators / D. F. Kornovan [et al.] // ACS Photonics. — 2021. — Vol. 8, no. 12. — P. 3627–3632.

37 Guiding optical modes in chains of dielectric particles / G. S. Blaustein [et al.] // Opt. Express. — 2007. — Vol. 15, no. 25. — P. 17380–17391.

38 Guided modes in the plane array of optical waveguides / I. Y. Polishchuk [et al.] // Phys. Rev. A. — 2017. — Vol. 95, no. 5. — P. 053847.

39 Zhang Y.-X., Mølmer K. Subradiant Emission from Regular Atomic Arrays: Universal Scaling of Decay Rates from the Generalized Bloch Theorem // Phys. Rev. Lett. — 2020. — Vol. 125, no. 25. — P. 253601.

40 Novotny L., Hecht B. Principles of Nano-Optics. — Cambridge, England, UK : Cambridge University Press, 2006. — ISBN 978-0-52153988-3.

41 Electrodynamics of continuous media. Vol. 8 / L. D. Landau [et al.]. — elsevier, 2013.

42 Babicheva V. E., Evlyukhin A. B. Multipole lattice effects in high refractive index metasurfaces // J. Appl. Phys. — 2021. — Vol. 129, no. 4.

43 Multipolar theory of bianisotropic response of meta-atoms / M. Poleva [et al.] // Phys. Rev. B. — 2023. — Vol. 107, no. 4. — P. L041304.

44 Achouri K., Martin O. J. F. Extension of Lorentz reciprocity and Poynting theorems for spatially dispersive media with quadrupolar responses // Phys. Rev. B. — 2021. — Vol. 104, no. 16. — P. 165426.

45 Weber W. H., Ford G. W. Propagation of optical excitations by dipolar interactions in metal nanoparticle chains // Phys. Rev. B. — 2004. — Vol. 70, no. 12. — P. 125429.

46 Petrov M. Disorder-induced Purcell enhancement in nanoparticle chains // Phys. Rev. A. — 2015. — Vol. 91, no. 2. — P. 023821.

47 Bloch F. ber die Quantenmechanik der Elektronen in Kristallgittern // Z. Phys. — 1929. — Vol. 52, no. 7. — P. 555–600.

48 Shore R. A., Yaghjian A. D. Complex waves on periodic arrays of lossy and lossless permeable spheres: 1. Theory // Radio Sci. — 2012. — Vol. 47, no. 02. — P. 1–16.

49 Shore R. A., Yaghjian A. D. Complex waves on periodic arrays of lossy and lossless permeable spheres: 2. Numerical results // Radio Sci. — 2012. — Vol. 47, no. 02. — P. 1–21.

50 Optical theorem and multipole scattering of light by arbitrarily shaped nanoparticles / A. B. Evlyukhin [et al.] // Phys. Rev. B. — 2016. — Vol. 94, no. 20. — P. 205434.

51 Evlyukhin A. B., Chichkov B. N. Multipole decompositions for directional light scattering // Phys. Rev. B. — 2019. — Vol. 100, no. 12. — P. 125415.

52 Tribelsky M. I., Miroshnichenko A. E. Giant in-particle field concentration and Fano resonances at light scattering by high-refractive-index particles // Phys. Rev. A. — 2016. — Vol. 93, no. 5. — P. 053837.